Available online at www.sciencedirect.com

SCIENCE DIRECT®

Biochimica et Biophysica Acta 1712 (2005) 109 – 127

BIOCHIMICA ET BIOPHYSICA ACTA
BBA

http://www.elsevier.com/locate/bba

Review

# Watching the components of photosynthetic bacterial membranes and their in situ organisation by atomic force microscopy

Simon Scheuring, Daniel Lévy, Jean-Louis Rigaud*

*Institut Curie, UMR-CNRS 168 and LRC-CEA 34V, 11 rue Pierre et Marie Curie, 75231 Paris Cedex 05, France*

Received 3 February 2005; received in revised form 4 April 2005; accepted 15 April 2005
Available online 5 May 2005

**Abstract**

The atomic force microscope has developed into a powerful tool in structural biology allowing information to be acquired at submolecular resolution on the protruding structures of membrane proteins. It is now a complementary technique to X-ray crystallography and electron microscopy for structure determination of individual membrane proteins after extraction, purification and reconstitution into lipid bilayers. Moving on from the structures of individual components of biological membranes, atomic force microscopy has recently been demonstrated to be a unique tool to identify in situ the individual components of multi-protein assemblies and to study the supramolecular architecture of these components allowing the efficient performance of a complex biological function.

Here, recent atomic force microscopy studies of native membranes of different photosynthetic bacteria with different polypeptide contents are reviewed. Technology, advantages, feasibilities, restrictions and limits of atomic force microscopy for the acquisition of highly resolved images of up to 10 Å lateral resolution under native conditions are discussed. From a biological point of view, the new insights contributed by the images are analysed and discussed in the context of the strongly debated organisation of the interconnected network of membrane-associated chlorophyll–protein complexes composing the photosynthetic apparatus in different species of purple bacteria.


*Keywords:* AFM; Photosynthesis; Purple photosynthetic bacteria; Light harvesting complexes; Reaction centre; Core complex; Photosynthetic unit; *Blastochloris viridis*; *Rhodospirillum photometricum*; *Rhodobacter blasticus*; *Rhodobacter sphaeroides*

**Contents**



*Abbreviations:* AFM, Atomic Force Microscopy; EM, Electron Microscopy; LH, light-harvesting; RC, reaction centre; 4Hcyt, tetraheme cytochrome; cyt *bc1*, Cytochrome *bc1* complex; PSU, photosynthetic unit; *Rb.*, *Rhodobacter*; *Rsp.*, *Rhodospirillum*; *Blc.*, *Blastochloris*; *Rvi.*, *Rubrivivax*; *Rps.*, *Rhodopseudomonas*

* Corresponding author. Tel.: +33 1 42346781; fax: +33 1 40510636.
*E-mail address:* rigaud@curie.fr (J.-L. Rigaud).

0005-2736/$ - see front matter © 2005 Elsevier B.V. All rights reserved.
doi:10.1016/j.bbamem.2005.04.005

## 1. Introduction

About 25% of the sequenced genomes of different eukaryotic and prokaryotic organisms are predicted to code for membrane proteins and an even larger fraction code for membrane-associated proteins [1]. This large fraction reflects the importance of membrane proteins which cover a wide spectrum of fundamental biological processes. The function, sequence and topology of many of these membrane proteins have been extensively studied. However, despite the important information obtained from biochemical, biophysical and molecular biology strategies, our understanding of membrane phenomena is severely hindered by a dearth of structural information. Indeed, as compared to soluble proteins, only few structures of membrane proteins have been solved by X-ray and electron crystallography (http://www.rcsb.org/pdb/; http://www.mpibp-frankfurt.mpg.de/michel/public/memprotstruct.html).

In this structural context, the atomic force microscopy (AFM) [2] has developed into a powerful tool in membrane protein research and is now a complementary technique to X-ray crystallography and electron microscopy (EM) [3,4]. The AFM is a remarkable instrument allowing high resolution topography of biological samples to be acquired near physiological conditions, i.e., in buffer solution at room temperature and under normal pressure [5–16]. Using the AFM, the heights of membranes and protruding structures can be measured accurately with a vertical resolution of ~1 Å [8,17,18]. The high signal-to-noise ratio of the instrument enables the oligomeric state and sidedness of membrane proteins directly to be assessed in raw data images [19–21] and poorly ordered single particles to be recognized and imaged at high resolution (~10 Å) [4,13,19–26]. The AFM has developed to the point that it permits now to detect flexible and stable extrinsic domains [18,27] and to perform time lapse AFM allowing identification of structural changes of molecules as a function of time [24,28–31]. Further, by applying loading forces to the AFM tip, biological samples can be nanodissected to give insights into protein assembly [21,30,32–36]. Finally, in addition to being used as a microscope, an AFM can measure biomolecular forces with piconewtons sensitivity. Using this method, known as force spectroscopy, a variety of inter- and intramolecular forces have been measured, including protein–protein interaction forces, unfolding forces and molecular recognition with specific antibodies [37–40]. Taking together, although the AFM will never provide an atomic structure due to its restriction to surface contouring, several examples demonstrate the capability of AFM to resolve characteristic substructures of single individual proteins, to study conformational changes, to analyse protein–protein interactions and the assembly of membrane proteins.

Most AFM reports have been related to single membrane proteins reconstituted into lipid bilayers as two-dimensional (2D) crystals or densely packed proteins [6,19–21,31,41,42]. Thus, as for X-ray and electron crystallographic approaches, AFM approaches require the difficult solubilisation, purification and reconstitution steps and are also limited by the high quantity of material required for structure determination. These limitations are even more crucial for the structural analysis of supramolecular complexes, in which different membrane proteins have to interact specifically to fulfil their physiological function. It is obvious that membrane protein structural biology is in need of a technique with a resolution high enough to identify the individual components of a multi-protein complex and to analyse their supramolecular organisation needed for relevant functions.

The last 2 years, high-resolution imaging of non-crystalline native membranes have been reported by AFM [30,43–47]. In particular, the value of this technique has been demonstrated in analysing the assembly of multi-component membrane protein complexes in native membranes of photosynthetic bacteria [30,43–46]. These anaerobic photosynthetic prokaryotes fuel their metabolism with light energy and have developed for this purpose a highly efficient photosynthetic apparatus consisting of a highly organised nanometric assembly of transmembrane protein complexes [48]. Absorption of light and its conversion into chemical energy require only four transmem-

brane protein pigments complexes localised in the intracytoplasmic membranes: a peripheral light harvesting complex LH2, a central light harvesting complex LH1 which complexes with the photochemical reaction centre (RC) and a proton translocating cytochrome *bc1* complex. The cascade of molecular events that follows the absorption of a photon has been determined in fine detail using time-resolved spectroscopy [49–51]. In addition, the protein constituents of the photosynthetic apparatus are structurally known by X-ray [52–59] and electron crystallography [60–69] and in the past years there have been a clutch of AFM studies looking at purified antenna complexes of different photosynthetic bacteria [18,20,70–73]. Despite all these functional and structural information, one of the main challenges relies on determining the organisation of the intact photosynthetic machinery and the basic requirement for the efficient harvesting, transmission and trapping of light energy. Thus, the purple photosynthetic bacteria offer a unique system for obtaining and integrating structural and functional information and are a paradigm for a protein complex assembly and for exploring in situ the general mechanisms of biological energy transduction.

Here, we review the experimental approaches that have allowed high resolution AFM imaging in situ of a assembly of multiple proteins functionally coupled and we give an introduction to the basic principles of how bacterial photosynthetic systems work, including structural, mechanistic and regulatory aspects. Then, we focus on the very recent results that show AFM to be of great interest for imaging specialised photosynthetic bacterial membranes. Emphasis will be placed on our current understanding of the highly efficient machinery involved in the conversion of sunlight into chemical energy and we will highlight some pressing issues that merit further investigation.

## 2. Atomic force microscopy (AFM)

### 2.1. Instrumentation

Key elements of an AFM instrument (Fig. 1a) are the cantilever with a pyramidal-shaped stylus that touches the sample, an optical lever consisting of a laser and a multi-faced photo-diode that allows to detect cantilever's deflections, a piezo-electric scanner that translates the sample relative to the tip in x, y, z directions and a computer that drives the microscope and stores the surface contours. The instrument can work under ambient condition in buffer solutions whose composition can be changed during the experiment (Fig. 1b). At this point, it is important to stress that all data presented in this review have been acquired in buffer solutions.

Atomic force microscopes can be operated in various modes. In the "constant-force imaging mode", images are created by bringing the tip and sample into contact and scanning the tip across the surface while the sample height

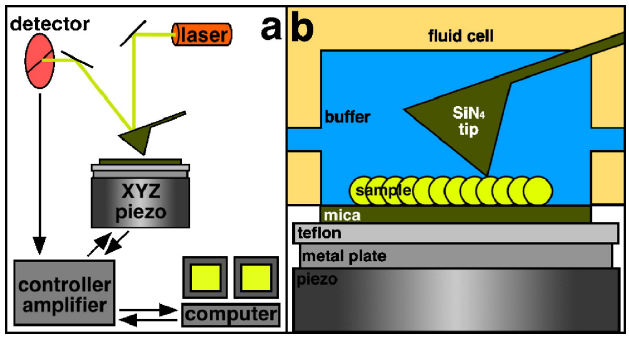


Fig. 1. Schematic representation of the AFM set-up. (a) A laser beam is deflected on the backside of the AFM cantilever monitoring the relative position of the cantilever on a multi-field detector. This signal is processed by the controller which drives the piezo in X- and Y-dimensions and compensates for the cantilever deflection through movements in Z-dimension. This compensation of the tip deflection by Z-movement of the piezo, which in turn will influence the tip deflection at each position (XY), is termed the feedback loop. The user interacts over a computer with the controller, feeds in the scanning parameters and reads out the piezo movements corresponding to the image, to and from the controller. The faster the feedback loop reacts, the more precise is the surface contouring of the sample. (b) Close-up view of the fluid cell. The sample is deposited on mica which is glued to a Teflon plate (protecting the piezo), which in turn is glued to a magnetic plate. The tip and the sample are permanently in buffer solution during the measurements.

is adjusted using a feedback loop to keep the deflection of the cantilever constant. This yields a topographic image that gives calibrated height information about the sample. The optical system resolves cantilever's deflections of 0.1 nm, which corresponds to a force difference of typically 10–50 pN. With modern instruments, stable contact mode operation is possible at forces of ~100 pN provided the sample is in an aqueous solution [74]. In the "oscillating mode", an oscillating tip is scanned over the surface and the amplitude and phase of the cantilever are monitored near its resonance frequency. As the tip touches the sample surface only at the very end of its downward movement, lateral forces during imaging are greatly reduced, which is advantageous for imaging soft biological samples.

### 2.2. Substrate–sample and sample–stylus interactions

Operating the AFM in contact mode induces frictions and samples need to adhere well to freshly cleaved mica substrates. Alternatively, friction forces can be minimised by using the "oscillating mode" which allows weakly adsorbed samples to be observed although at a reduced resolution [7,75–82].

As demonstrated using a variety of biological samples with different surface charge densities [74,83–86], sample adsorption is controlled by the nature and concentration of electrolytes in the buffer solution [87–89]. The interactions between the sample and the stylus involve to a large extent the same forces that occur between sample and support, i.e., electrostatic and Van der Waals forces (Fig. 2a) [74]. Immobilization therefore requires different buffer conditions than imaging. For adsorption, the Debye layer thickness

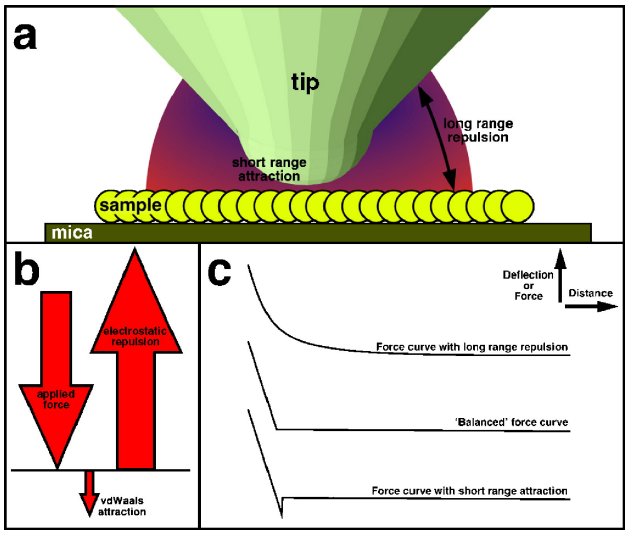


Fig. 2. Tip-sample interaction in a fluid cell. (a) Schematic representation of the AFM tip interacting with the sample. The tip pyramid interacts with a large sample area through electrostatic repulsions over large distances. At the same time, the tip apex interacts at very short distances with the sample. (b) Vector representation of the contributions of long-range electrostatic repulsions and short range Van der Waals attractions together with the force applied to the tip. In ideal cases, the force applied does not exceed ~100 pN and will nullify with the other interaction forces present. (c) Schematic representation of force-distance curves found on biological objects. Top: force curve in which long-range repulsive forces predominate. The cantilever deflects at large distances from the surface. Middle: ideal force curve for high-resolution imaging. The forces are 'balanced' to yield a zero-force baseline until physical contact with the object is established. The feedback loop will properly react on cantilever deflection using minimal forces applied. Bottom: at short distances from the surface, attractive forces are present. This interaction will constantly pull the tip into the sample, causing destruction of the biological sample.

needs to be minimised to allow adsorption by Van der Waals attraction [87]. For imaging, the electrolyte should be selected to balance electrostatic repulsions and Van der Waals attractions [74]. These forces can be quantitatively described and recording conditions optimised (Fig. 2b and c).

Significant progress have been achieved in many laboratories by optimising sample preparation (stable sample supports, buffer composition to control the substrate–sample and sample–stylus interactions) and imaging conditions of soft biological material (force–distance curves to adjust the forces applied to the cantilever below 100 pN, calibration of the scanning speed and feed back parameters).

### 2.3. Imaging

A crucial parameter for AFM imaging is the flatness of the adsorbed membrane or how tight the object is adsorbed. Native membranes are often vesicular. Non-flatly adsorbed membranes or not completely collapsed vesicles can present multiple technical problems and forces applied might be wrongly estimated. Vesicular structures can be vertically 'squeezed' when the tip pushes onto a not-tightly-attached region. This can be observed in forces–distance curves which exhibit faint repulsion over relatively large distances from the actual point of contact. As a consequence, the 'squeezing' of the object contributes to the apparent spring constant and the feedback-loop monitoring the tip deflection will not drive the piezo appropriately to gain a highly contrasted image. Furthermore, membranes that are not tightly attached can provoke 'smeared' images, probably due to faint displacement of the membrane during scanning, at least in contact mode imaging. Such 'smearing' can resemble piezo creep but can be distinguished since 'smearing direction' follows the scan line direction while piezo creep marks a uniform distortion in trace and retrace images.

Other crucial parameters for AFM imaging are related to the physics of the surface contouring mechanism employed, i.e., the feedback loop, but also to the mobility of membrane protruding protein structures, which increases with increasing length of protruding domains. For both reasons, one generally expects the contouring precision to decrease with increasing height of surface protruding structures. When strongly protruding globular domains are imaged, the tip geometry, in a first approximation, a hemi-sphere with a defined radius, convolutes the topography significantly: the height measurement of a strongly protruding domain can be precise but the diameter measurement appears enlarged due to tip convolution. While the topographies of weakly protruding protein domains (<2 nm) compare well with surface representations calculated from high-resolution structures [4], it seems unreasonable to interpret structural details of large globular topographies. The problem becomes even more pronounced when the tip geometry deviates from the shape of a hemi-sphere. This phenomenon, called 'asymmetric tip' or 'double tip' [90], can interfere with reliable contouring ranging from submolecular details to globular structures of several nanometres. This effect makes difficult the analysis of non-oligomeric molecules (in particular in native membranes where no regular lattice or crystallographic symmetry can be used to estimate tip symmetry) or of molecules for which no alternative structural information is available.

Another aspect of the imaging mechanism is the non-homogeneous resolution within one AFM topograph. As a logical consequence of the tip convolution and the feedback system, the imaging resolution within one AFM topograph is not identical on all points of an image. For example, one can imagine a situation where a weakly protruding highly resolved particle is in proximity to a globular structure strongly subjected to tip convolution and to non-precision of contouring. In this situation, regions directly beside a strongly protruding domain must structurally be considered as 'fantasy' since the contour recorded represents the edge of the tip sliding down the neighbouring globular structure rather than the tip apex being in contact with the underlying surface. All these considerations are true when considering the apex of the tip being in physical contact with the object. The situation gets more complex when considering particular physicochemical surface properties to interfere at each tip-sample contact point [86,91].

Another crucial limitation for high-resolution AFM topographs is related to the tip radius. It has to be stressed that, while suppliers specify tip radii of 10–50 nm, topographs of flat biological surfaces can be acquired at subnanometre resolution. Therefore, the tips employed most likely have a nanometre-sized asperity that protrudes sufficiently to contour the finest surface structures. Barrel-shaped molecules with small diameters, like light-harvesting complexes LH2 [18,20,73], represent an ideal system to estimate the AFM tip radius (Fig. 3). In a first approximation, the LH2 is considered as a perfect open cylinder with a diameter $D$ of 50 Å and the tip as a hemisphere with an apex radius $r$ to be determined. When the tip is positioned centrally over the LH2 ring, it will penetrate as far as possible into the cylinder with the obvious rule that a sharper tip can enter more deeply into the barrel-shaped molecule than a blunt tip (Fig. 3a). As long as the measurable depth $d$ is inferior to the total height $h$ and half of the diameter $D/2$ of the barrel-shaped molecule, it can directly be used as a measure to estimate the tip radius $r$, giving $r = \sqrt{(D/2)^2 + (r-d)^2}$, resulting in $r = D^2/8d + d/2$ (Fig. 3b).

Taking into account that an organised buffer layer covers the barrel boarders of the molecule, the actual barrel that the tip interacts with is probably narrower than the structure itself. Consequently, the resulting tip radius calculation represents a 'large estimate'. From the data obtained on the LH2 complexes from different photosynthetic bacteria [18,20,44,73] and the above-described considerations, we can calculate that the high-resolution AFM tips have a radius of ~2.5 nm. The time consuming process of finding a tip with such a sharp apex can be considered as another limitation for high-resolution AFM imaging of proteins.

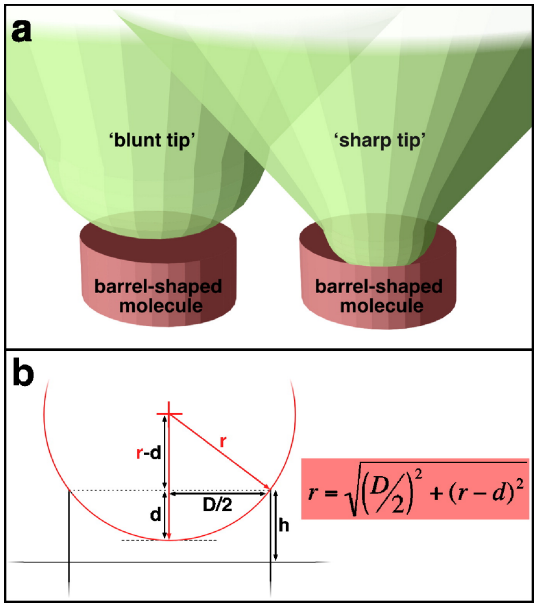


Fig. 3. Geometric considerations and tip radius. (a) Schematic representation of a 'blunt tip' and a 'sharp tip' positioned over a barrel-shaped molecule. A 'sharp tip' can penetrate into the centre of the barrel-shaped molecule more profoundly that a 'blunt tip'. (b) Outline and formula showing how to calculate the tip radius (r) from depth (d) and diameter (D) measurement on a barrel-shaped molecule.

### 2.4. Resolution of AFM imaging on membranes

The AFM can provide directly atomic resolution on solid crystalline surfaces such as mica or graphite [2,92]. On lipid bilayer containing membrane proteins, imaging resolution in buffer solution is most probably limited due to protein motion at room temperature. High-resolution images are acquired at scan speeds around 1 ms/nm [19–21,24,30,74]. It seems reasonable to assume that some protein motion is averaged during this time scale, limiting the acquisition of more detailed structural information. However, due to the high signal-to-noise ratio in AFM topographs, it was proven through comparison with atomic models derived from X-ray analysis that subnanometre resolution could be acquired, contouring individual beta-turns and loops connecting transmembrane α-helices [4].

It is also important to note that standard image averaging techniques have proved useful both to interpret the structural appearance of a protein and to assess the resolution attained. Common structural details of the individual proteins are enhanced in such averages while variable features are suppressed. However, the variable structural regions of the proteins are clearly identified by the simultaneously calculated standard deviation and can be studied in raw data, with the problem that variability might be due to imaging noise. Briefly, averages of complexes are calculated from trace and retrace images acquired at different magnifications using single particle analysis program packages and a reference-free alignment procedure [93,94]. Averaging allows the resolution of the averages to be determined using the signal-to-noise criterion [95,96] and average images are filtered at the computed resolution.

Topographs of membrane proteins at subnanometre resolution were first acquired on highly ordered 2D-crystals [6,35,41]. Then, technical barriers have been overcome and high-resolution images could be acquired on non-crystalline reconstituted membrane proteins [19–22,24,42]. This has opened the AFM analysis to membrane proteins directly in native membranes. As demonstrated recently for the analysis of bacterial photosynthetic membranes, it seems obvious that the AFM will become a key technique for the in situ investigation of integrated membrane protein assemblies and will play an important role in the elucidation of the structural organisation of native cytoplasmic membranes.

## 3. The photosynthetic apparatus of purple bacteria

### 3.1. Functional aspects: Photo-induced cyclic electron transfer

All green plants, algae and certain bacteria can convert the radiant energy supplied by the sun in chemical energy.

The process by which this transformation of energy is carried out is called photosynthesis. Photosynthetic organisms are grouped in 2 classes, oxygenic [97] and anoxygenic [98]. Higher plants, algae and cyanobacteria perform oxygenic photosynthesis, which involves reduction of $CO_2$ to carbohydrate and oxidation of water to produce molecular oxygen. Some photosynthetic bacteria, such as purple bacteria, carry out anoxygenic photosynthesis, which involves oxidation of molecules other than water. In spite of these differences, the general principles of energy transduction and the molecular machinery involved in the initial steps of photosynthesis are very similar in plant and bacterial photosynthesis. Purple bacteria are the model system for this process and the last 50 years have seen tremendous progresses in our understanding of the reactions taking place in these species. This complex subject cannot be adequately covered in this review and the interested readers are referred to other reviews in which various aspects of photosynthesis are explained in more details [48–51,99–101].

The conversion of light into chemical energy begins with the absorption of a photon by light harvesting (LH) complexes (Fig. 4a). To ensure an efficient collection of light energy, the purple bacterial antenna system is typically made up of two types of light-harvesting complexes, commonly referred as B800–B850 (LH2) and B875 (LH1) complexes according to their in vivo absorption maxima. The amount of LH2 is modulated by several factors such as light intensity and oxygen partial pressure whereas the LH1 complement is synthesised in fixed stoichiometry with the reaction centre (RC), forming the so-called LH1–RC core complex. After a photon is absorbed by the LH complexes, the excitation is funnelled toward a special pair of bacteriochlorophylls (BChls) in the RC in less than 100 ps and charge separation occurs. The energy is used for the release of an electron, which is transferred to a bacteriopheophytin molecule (Bphe) in 2 ps, then to the primary quinone acceptor QA in 200 ps and subsequently to the secondary ubiquinone QB. After a second turnover, the doubly reduced QB picks up 2 protons from the cytoplasmic space and is then released from the RC. The QH2 quinol formed is oxidized by cytochrome (cyt) c2, a reaction catalysed by the membrane protein cytochrome *bc1* complex (cyt *bc1*) which releases 2 protons in the periplasmic space. The cyclic electron transfer is completed by the reduction of the photooxidized primary electron donor by cyt c2. Thus, the cyclic electron transfer is coupled to the translocation of protons from the cytoplasm to the periplasm and the net result of this process is the formation of an electrochemical gradient for proton. This so-called proton motive force can then fuel the phosphorylation of ADP to ATP by the $F_0F_1$ ATP synthase.

Thus, in bacterial photosynthesis, light harvesting and subsequent cyclic electron transfer relies on the interplay between only four protein pigments complexes: a peripheral light harvesting complex LH2, a central light harvesting complex LH1 which complexes with the photochemical reaction centre RC and a proton translocating cyt *bc1* complex. The total system comprising the multi-protein assembly of multiple LH2s and LH1–RC core complexes is termed the 'photosynthetic unit' (PSU).

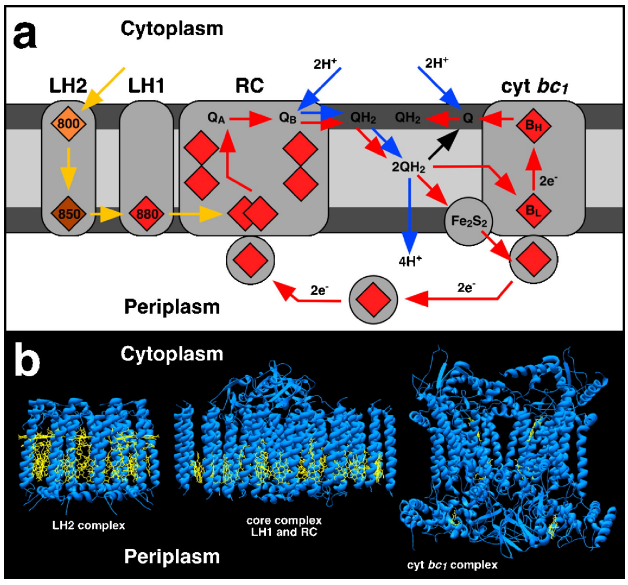


Fig. 4. Functional and structural aspects of bacterial photosynthetic membranes. (a) Schematic representation of the photo-induced cyclic electron-transfer chain in photosynthetic bacteria (adapted from [131]). Diamonds represents pigment molecules. The yellow arrows represent excitation transfer; the red and blue arrows correspond to electron and proton transfer, respectively. After absorption of a photon by the light harvesting complexes (LH1 and LH2), the excitation reaches the reaction centre (RC) where charge separation occurs. An electron is transferred from the excited primary donor of the RC to the secondary acceptor QB via a molecule of bacteriopheophytin and to the primary quinone, QA. After a second turnover, the doubly reduced QB picks up two protons from the cytoplasmic space. The quinol (QH2) formed is oxidized by cyt c2, a reaction catalysed by the cytochrome *bc1* complex which releases two protons to the periplasmic space. The cyclic electron transfer is completed by the reduction of the photooxidized primary electron donor by cyt c2. (b) 3D structures of the different components of the photosynthetic apparatus. From left to right: LH2 of *Rps. acidophila* structure [58, 59], LH1–RC core complex *Rps. palustris* [56], Cyt *bc1* complex from mitochondria [57].

### 3.2. Structural aspects

Tremendous progresses in our understanding of bacterial photosynthesis have been achieved with the determinations of the structures of the different components of the photosynthetic apparatus (Fig. 4b).

#### 3.2.1. Reaction centre

The determinations of the 3D structures of the RC of *Blastochloris* (*Blc.*) *viridis* and shortly after of *Rhodobacter* (*Rb.*) *sphaeroides* have provided an unprecedented opportunity to understand the function of photosynthetic reaction centres [52,53,102–105]. The membrane spanning RC is a 101-kDa heterotrimer consisting of the protein subunits L, M and H. The L and M subunits have a molecular weight of

31 and 34 kDa and each contains 5 membrane-spanning helices. The H subunit crosses the membrane only once and has a mass of 28 kDa. For *Blc. viridis*, a non-membranous tetraheme cytochrome (4Hcyt) was found topping the RC on the periplasmic side. The RC contains 10 co-factors including one critical carotenoid, 2 Bphe molecules and 4 BChl molecules, two of which forming the primary donor P870.

### 3.2.2. LH antenna complexes

Different types of LH antenna complexes have been isolated from various species of purple bacteria and their structures solved at high resolution. The basic unit is a heterodimer consisting of two small polypeptides α and β, which both span the membrane once as a transmembrane helix. An aggregation of these heterodimers in a ring gives the tertiary structure of the complex which appears as a hollow cylinder. The inner walls of the cylinder are formed by the α-apoproteins and the outer walls are formed by the β-apoproteins. Within these protein walls are located the pigment molecules, three Bchla and two carotenoids.

Concerning the light harvesting complex LH2, McDermott et al. (1995) first solved the atomic structure of the LH2 from *Rhodopseudomonas* (*Rps.*) *acidophila* by X-ray crystallography, revealing a membrane-spanning cylinder formed by nine αβ-heterodimers [58]. Later, the atomic structure of LH2 from *Phaeospirillum molischianum* revealed a very similar structure with the notable difference that it was an octamer [55]. In this 9- or 8-mers context, more recent EM data and high resolution AFM topographs were acquired on two-dimensional crystals of LH2s from *Rhodovulum sulfidophilum* [106], *Rb. sphaeroides* [18,62], *Rubrivivax* (*Rvi.*) *gelatinosus* [20,63], all exhibiting a nonameric organisation.

Concerning the light harvesting complex LH1, its structure is still unknown at atomic resolution. An EM projection map at 8.5 Å resolution of *Rhodospirillum* (*Rsp.*) *rubrum* LH1 in the absence of the RC showed a circular ring-like structure similar to that reported for LH2s complexes but consisting of 16 αβ-heterodimers [60]. As the authors pointed out, the hole in the middle (68 Å inner diameter) was sufficient to accommodate a RC, in agreement with early electron microscopy studies of native membranes of *Blc. viridis* containing regular arrays of RC–LH1 complexes with the RC clearly located inside the LH1 ring [107]. Although a higher resolution structure is still required, many recent structural studies of the LH1–RC core complexes from different species have provided valuable information to elucidate the detailed molecular architecture of LH1 (see below).

### 3.2.3. LH1–RC core complex

No atomic level structure of the LH1–RC core complex is available and its structure is strongly debated. However, data of different core complexes at resolution sufficient to delineate the LH1 assembly around the RC are available: a cryo-EM projection map at 8.5 Å resolution of *Rsp. rubrum* [66], an AFM topography at 10 Å resolution of *Blc. viridis* [30] and an AFM topography at 15 Å resolution of *Rb. blasticus* [43]. At highest resolution, a 3D-structure at 4.8 Å resolution of the core complex of *Rps. palustris* is available, revealing the backbone of the peptides [56]. Taking together, the core complex was described to consist of a RC surrounded by an ellipse of either 16 LH1 α/β heterodimers (*Rsp. rubrum*, *Blc. viridis*) or 15 LH1 α/β heterodimers plus a poorly characterized W (PufX-like) peptide (*Rps. palustris*), or as a dimer consisting of two RCs surrounded by an S-shaped LH1 assembly constituted of two times 13 LH1 α/β heterodimers plus 2 PufXs (*Rb. blasticus*). Considering all these structural data, we have to accept the idea that core complexes from different species have different polypeptide compositions and different architectures.

Despite the diversity in the architecture of the core complex among species, all structural information agree now in the point that the LH1 assembly, with or without interplay of an additional polypeptide (PufX or W), forms an ellipsis around the RC with a ~10% length difference of the long and the short ellipsis axes. This issue has been debated for a long time since, depending upon the crystallization conditions and/or the bacterial origin of the core complex, square-shaped, ellipsoid or round architectures of the LH1 subunits around the RC have been proposed. Today, a circular LH1 assembly in presence of the RC seems definitely ruled out by the overwhelming structural information obtained by AFM data on native membranes, i.e., in which non-crystalline core complexes have not been exposed to detergent effects and were solely housed in their native in vivo environment [30,43–45].

### 3.2.4. Cytochrome bc1

The structures of the homologous cytochrome *bc1* complex from mitochondria [57] and of the cytochrome *b6f* complexes from cyanobacteria and algae have been solved [108,109]. All structures show a dimeric arrangement with an overall size of ~5 nm × ~10 nm perpendicular to the membrane plane. A very recent preliminary X-ray structure of the cyt *bc1* from *Rb. capsulatus* [110] indicates an intertwined homodimer with the 2 monomers organised around a 2-fold axis, as previously reported for the mitochondrial and the chloroplast enzymes. The number of the transmembrane helices of the three subunits composing the complex is eight for cytochrome *b*, one for the high potential 2Fe-2S Rieske protein and one for cytochrome *c*1. The cytochrome b subunit, which contains two b-type hemes, serves as the central core of the complex on which other subunits are bound and makes the wall of the quinone binding sites. On the periplasmic side, the hydrophilic part of the Rieske and cyt c1 subunits protrudes by about 35 Å. Noteworthy, the massive core proteins strongly protruding on the cytoplasmic side in the mitochondrial cyt *bc1* do not exist in photosynthetic bacteria.

### 3.3. Organisation of the photosynthetic apparatus

Despite the wealth of functional and structural information available on the individual membrane proteins, their supramolecular organisation in the bacterial photosynthetic membrane is still poorly understood. Numerous models of a bacterial photosystem have been proposed to explain its enormous efficiency of >95% but they are still matter of debate [48,51,111–113]. Moving on from the structures of individual components, it is thus necessary to describe and understand their higher order molecular assembly in the membrane in order to learn how these structures allow the efficiency of a complex biological function. Very recently, the AFM has proven to be a key technique for the investigation of the photosynthetic apparatus in native membranes. In the following part of this review, the recent structural AFM data of the architectures and interplays between the photosynthetic proteins are reviewed. From these data, novel insights into the LH2 assembly, the core complex architecture and the lateral arrangement of the different complexes could be gained.

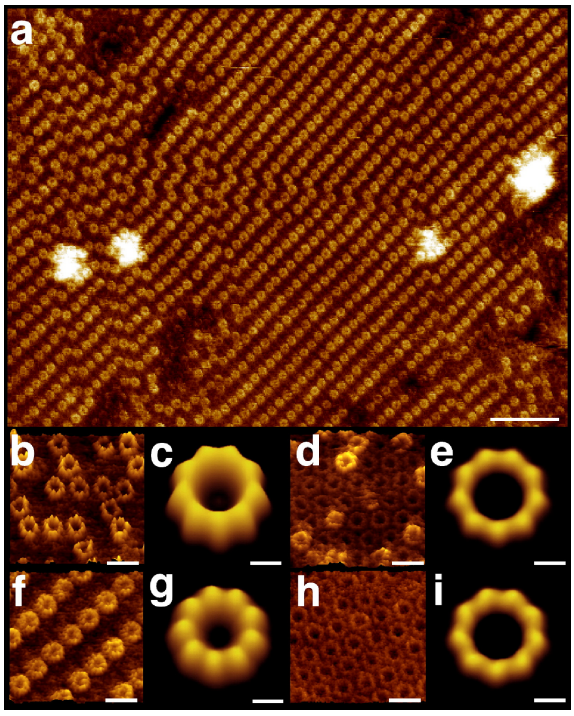


Fig. 5. AFM images of *Rubrivivax gelatinosus* LH2 complexes. High-resolution topography analysis of reconstituted *Rvi. gelatinosus* LH2 2D crystals (adapted from [20]). (a) Medium resolution AFM topograph of a reconstituted LH2 2D crystal showing areas of crystallinity interspaced by more randomly LH2 packed domains. Scale bar: 50 nm. (b) Raw data topograph of the periplasmic surface of the LH2 complex. Scale bar: 10 nm. (c) Average of the periplasmic surface. Protrusion height: 16 Å. Scale bar: 2 nm. (d) Raw data topograph of the cytoplasmic surface of the LH2 complex. Scale bar: 10 nm. (e) Average of the native cytoplasmic surface. Protrusion height: 5 Å. Scale bar: 2 nm. (f) Raw data topograph of the periplasmic surface of the proteolysed LH2 complex. Scale bar: 10 nm. (g) Average of the proteolysed periplasmic surface. Protrusion height: 9 Å. Scale bar: 2 nm. (h) Raw data topograph of the cytoplasmic surface of the proteolysed LH2 complex. Scale bar: 10 nm. (i) Average of the proteolysed cytoplasmic surface. Protrusion height: 5 Å. Scale bar: 2 nm.

## 4. High resolution AFM imaging of photosynthetic complexes

### 4.1. Individual proteins in 2D crystals

In the recent years, there have been many AFM studies looking at individual components of the photosynthetic apparatus after solubilisation, purification and reconstitution into 2D crystals. They have allowed LH2, LH1 and LH1–RC complexes from different species to be imaged at high resolution. To produce 2D crystals of these complexes, the general method [114,115] has consisted to start with the purified proteins and a suitable combination of lipids, both solubilised in detergent. Next, the detergent has been removed by dialysis or by hydrophobic adsorption onto polystyrene beads resulting in the formation of lipid bilayers in which the proteins were reconstituted as 2D crystals or densely packed proteins.

The first demonstration of the usefulness of AFM in the field of photosynthetic bacteria was an investigation of LH2 from *Rvi. gelatinosus* (Fig. 5) [20]. The most distinct feature of this antenna complex is related to the sequence of the α-polypeptide chain which has a C-terminal extension that is 21 amino acids longer than the C-terminus of α-subunits from other species. As proposed on the basis of its hydrophobicity, this extension could be folded into a transmembrane helix, leading to a α-subunit spanning the membrane twice in a hairpin structure [116]. A comparison of the electron microscopy projection maps from 2D crystals of native or truncated (thermolysin-treated) *Rvi. gelatinosus* LH2 did not allow any extra density to be detected inside or outside a nonameric ring of the αβ-heterodimers and the location of the C-terminal extension could not be identified [63]. Interestingly, high-resolution AFM imaging of the 2D crystals with an 'up and down' insertion of LH2 complexes revealed a significant change of the surface appearance upon thermolysin treatment. Native LH2 showed one surface protruding from the membrane by 16 Å (Fig. 5b and c) and the other protruding by 5 Å (Fig. 5d and e). Upon thermolysin treatment, the height of the strongly protruding surface was reduced to 9 Å (Fig. 5f and g) while the weakly protruding surface showed an identical appearance (Fig. 5h and i). This allowed the periplasmic surface to be assigned and an unambiguous identification of the extrinsic C-terminal domain of the α-polypeptide, ruling out the model of a buried transmembrane C-terminus [20]. Such data evidenced the complementarities of AFM and EM studies and illustrated the powerful of AFM in analysing with a high precision the oligomerisation of light harvesting complexes but also the protrusion heights and intrinsic flexibilities of their individual subunits.

Following this study, several AFM reports have analysed the light harvesting complexes from other bacteria. For example, AFM was found to be very powerful in analysing the tilt of LH2 complexes with respect to the membrane plane. AFM topographs of 2D crystals of *Rb. sphaeroides* LH2 complexes demonstrated that the nonameric cylinder-shaped complexes could be inserted with a tilt with respect to the membrane plane (Fig. 6a). A detailed analysis of the protrusion heights of the different subunits (maximal and minimal protrusion heights of 13.1 Å and 3.8 Å, respectively) revealed that the whole LH2 complex was tilted 6.2° with respect to the membrane plane. However, a further AFM study of *Rps. acidophila* LH2 complexes reconstituted in different 2D crystals forms indicated that a tilted insertion of the cylinders was dependent upon specific protein–protein contacts and could not reflect the native state of the complex (Fig. 6b and c) [73]. These results pointed out the need of AFM analysis of native photosynthetic membranes before a final interpretation of a membrane protein tilt.

Concerning the light harvesting complex LH1, an AFM analysis of 2D crystals of *Rb. sphaeroides* LH1 complexes has shown large variations from molecule to molecule in terms of both shape and size [72]. Circles, polygonal rings, open rings, ellipses and more anomalous structures such as arcs were all observed (Fig. 7a and b). These data led to the conclusion that the LH1 ring was intrinsically highly deformable and provided a direct visualisation of the consequences of the relatively weak associations that govern the association of the $Bchl_2$ protomers comprising the LH1 complex. This implied flexibility was suggested to be a significant factor in the export of quinol from the RC to the cyt *bc1* complex. However, a definite interpretation has to take into account that the absence of the RC complex may deprive the assembly system of a guide or template, on which LH1 is assembled. Furthermore, lateral packing forces exerted in 2D crystals can distort the LH1s as observed by electron microscopy for *Rsp. rubrum* RC–LH1 complexes which assemble into circles or ellipses depending on whether the crystal form is tetragonal or orthorhombic, respectively [66]. Finally, 2D crystals are produced from detergent-solubilised complexes, raising the question of whether solubilisation, purification and/or reconstitution into specific lipids lead to intact complexes without loss or rearrangement of small subunits.

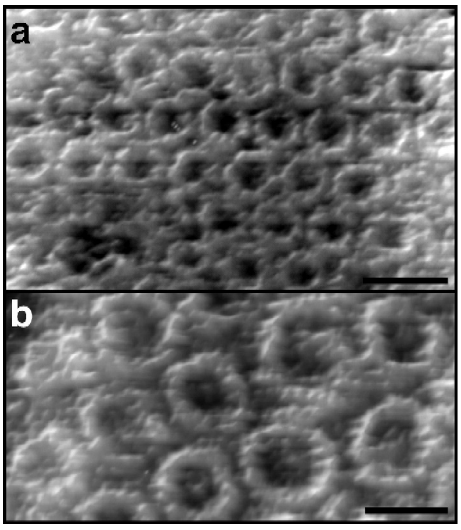


Fig. 7. AFM images of *Rhodobacter sphaeroides* LH1 complexes. High-resolution topography analysis of reconstituted *Rb. sphaeroides* LH1 2D crystals (adapted from [72]). (a) Low magnification AFM topograph of a reconstituted *Rb. sphaeroides* LH1 hexagonal 2D-crystal (Scale bar: 20 nm). (b) High magnification AFM topograph displaying the variability in shapes and sizes of LH1 complexes (scale bar: 10 nm).

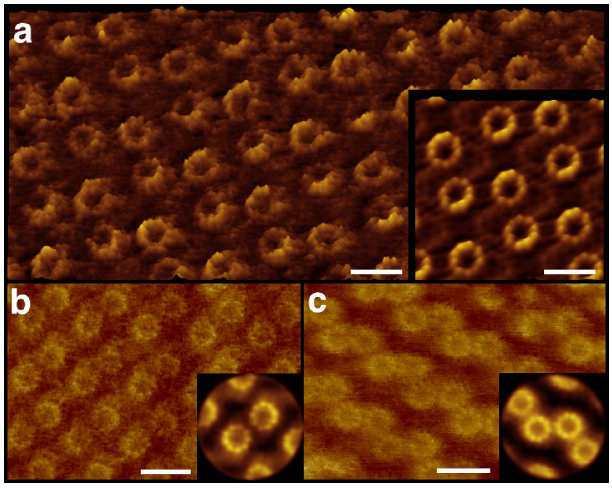


Fig. 6. AFM images of *Rhodobacter sphaeroides* and *Rhodopseudomonas acidophila* LH2 complexes (a) Raw data AFM topograph of a reconstituted *Rb. sphaeroides* LH2 2D-crystal (adapted from [18]). The tilted integration of the LH2 is clearly visible by the uneven height distribution of the ring surface. Inset: average topography of the LH2 2D crystal. In this crystal packing, the unit cell contains 2 molecules in 'up' and 2 molecules in 'down' orientation. The molecules are tilted by 6° with respect to the membrane plane. Scale bar: 10 nm. (b and c) Raw data AFM topograph of different 2D crystal forms produced from *Rps. acidophila* LH2 complexes at different lipid to protein ratios (adapted from [73]). (b) topograph of a type I 2D-crystal I which the LH2 cylinders are tilted with respect to the membrane plane. (c) topograph of a type II 2D crystal in which the LH2 cylinders are not tilted with respect to the membrane plane. Scale bar: 10 nm. Insets: averages.

Concerning the LH1–RC core complex, high resolution AFM topographs recorded from 2D crystals of purified *Rsp. rubrum* core complexes showed a closed ring of αβ subunits around the central RC density (Fig. 8) [71]. Taking advantage of an 'up and down' orientation of the complexes in the reconstituted 2D crystals, both periplasmic and cytoplasmic surfaces of the LH1–RC could be imaged at high resolution. Furthermore, nanodissection by the AFM tip removed the RC-H subunit allowing to image the underlying RC-L and M-subunits. LH1s completely lacking RCs were also found. This study made possible to measure directly the position of the membrane–water interface in relation to RC–LH1 chromophores and aromatic residues. These AFM measurements have been reconciled with previous EM and NMR data to produce a model of the

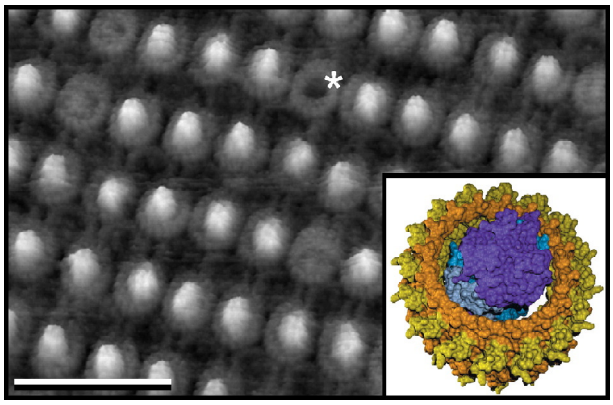

Fig. 8. AFM images of *Rhodospirillum rubrum* LH1–RC core complexes. High resolution AFM topograph of reconstituted *Rsp. rubrum* LH1–RC 2D crystals (adapted from [71]). The crystal is composed of alternating rows of complexes in 'up and down' orientations, exposing either the strongly protruding cytoplasmic side (bright rows) or the low periplasmic side (dark rows). The asterisk denotes "empty" LH1 complexes lacking the RC (scale bar: 40 nm). Inset: model of the RC–LH1 complex of *Rsp. rubrum*.

RC–LH1 core complex (inset Fig. 8). However, an intriguing observation that emerged from AFM and EM [66] studies was that the LH1 ring, in the presence or absence of RC, could adopt a large variety of architectures: circular, elliptical, "D" or "angular "shaped" forms could be visualised, depending dramatically on external packing constraints. When these packing forces are evenly applied as in tetragonal 2D crystals, complexes were circular [66,71]. In contrast, when packing forces are anisotropic as in orthorhombic crystals, complexes could be squeezed and adopted an elliptical shape. All these data brought important structural features on the architecture of the core complexes but, again, pointed out the need of AFM analysis of native photosynthetic membranes for a final interpretation of the antenna architecture.

### 4.2. Protein assembly in native membranes

The images now being produced by AFM on the individual components of the bacterial photosynthetic apparatus are spectacular. Interestingly, all the AFM data reported above provide the opportunity to obtain high signal-to-noise data without the need to obtain highly ordered 2D crystals. This has opened the way to use the AFM technology to map the structure of individual proteins and their supramolecular organisation in situ within intact photosynthetic membranes.

#### 4.2.1. Preparation of photosynthetic bacterial intracytoplasmic membranes

Cell fractionation techniques and density gradient purification established that the major portion of the photosynthetic machinery of anoxygenic photosynthetic bacteria could be isolated as a discrete fraction. Ultrastructural observations of these pigmented particles, designed as chromatophores, showed that they arose from internal vesicular, tubular or lamellar structures of different cellular organisation. The term "chromatophores" was replaced with the more general and descriptive term, intracytoplasmic membranes (ICM), since they originate from invagination of the cytoplasmic membrane or preformed intracytoplasmic vesicles rather than de novo [117]. Using freeze-fracture electron microscopy, a pattern of regularly arranged 10 nm intramembrane particles was observed in the ICM of *Blc. viridis* while the fracture faces of *Rhodospirillum*, *Rhodobacter* and *Rhodocyclus* species were densely packed with particles of varying sizes [107,118,119].

For intracytoplasmic membrane preparation, bacterial cells are first broken by multiple passages through a French pressure cell. Then the lysates are loaded directly onto sucrose gradients and centrifuged. The isolated ICM membranes are dialysed against a sucrose free buffer before AFM analysis. If the sizes of the purified ICM are too small for AFM imaging, freeze–thaw cycles [30,43] or sub-solubilising detergent treatment [46] have been used to induce membrane fusion.

#### 4.2.2. The PSU of Blastochloris viridis

*Blc. viridis* is a bacterium which has no LH2 and a low number of cytochrome *bc1*. The particular hexagonal packing of the RC–LH1 core complexes in its chromatophore membranes was discovered and analysed early [64,65,107]. Projection maps at low resolution reported the overall architecture of the core complex with a RC surrounded by a fence of closely associated LH1 subunits. As we know now, the hexagonal 'crystal' packing follows only the rules of densest packing of roundish complexes and hampered the elucidation of the subunit architecture by electron crystallography [67,120,121]. This limitation has been alleviated using AFM to image the core complexes in situ at high resolution.

After membrane purification, the small chromatophores of *Blc. viridis* were fused by freeze thawing to allow their imaging by AFM. The resolution and the signal-to-noise ratio of the raw data AFM images presented were sufficiently high to visualise individually the small LH1 subunits, revealing the oligomerisation, the architecture and the intermolecular interactions between the subunits of the core complexes, which were solely housed in their in situ environment (Fig. 9a) [30].

In *Blc. viridis*, the RC consists of the (L), (M), (H) and the tetraheme cytochrome (4Hcyt) subunits, and the LH1 of the α and β-polypeptides. High resolution images of firmly adsorbed membranes revealed a vertical resolution of ~1 Å and a lateral resolution of 10 Å as judged from spectral signal-to-noise analysis gained through single particle averaging. The complete core complex $4Hcyt_{(1)}$–RC $(L,M,H)_{(1)}$–$LH1(\alpha,\beta)_{(16)}$ reveals the LH1 topography and dominantly the strongly protruding tetraheme cytochrome associated to the RC (Fig. 9b1). This subunit is contoured as a globular structure with a height of 48 Å over the membrane and a diameter of ~50 Å. In spite of a 10%

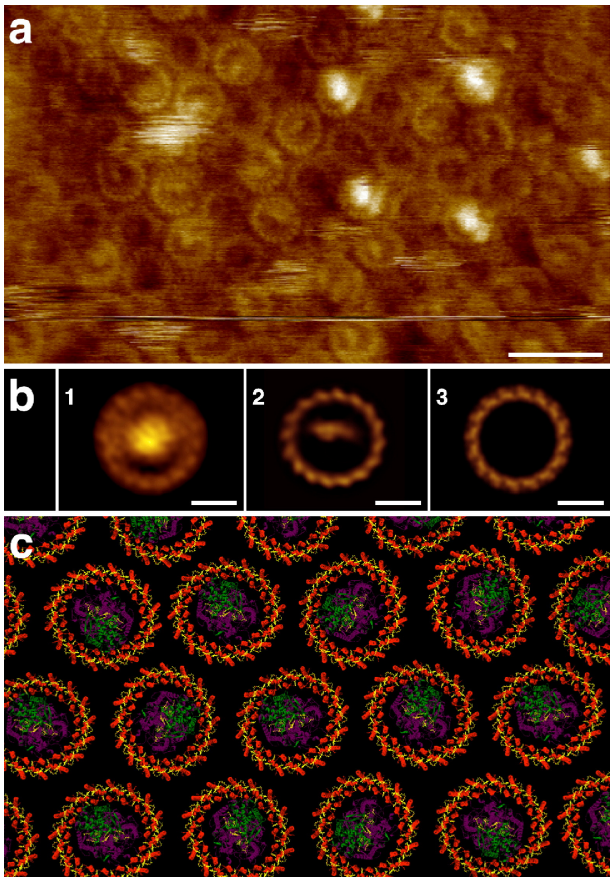


Fig. 9. AFM Images of the native membrane of *Blastochloris viridis.* High resolution AFM analysis of the native photosynthetic membrane of *Blc. viridis* (adapted from [30]). (a) Raw data AFM topograph of hexagonally packed core complexes in the native photosynthetic membrane of *Blc. viridis*. Scale bar: 20 nm. (b) Nanodissection using increased loading forces to the AFM stylus allows imaging, extraction and averaging of three classes of protein complexes: (1) $4Hcyt_{(1)}$–RC $(L,M,H)_{(1)}$–$LH1(\alpha,\beta)_{(16)}$; (2) RC $(L,M,H)_{(1)}$–$LH1(\alpha,\beta)_{(16)}$; (3) $LH1(\alpha,\beta)_{(16)}$. Scale bar: 5 nm. (c) Model of the complex assembly in the native membrane of *Blc. viridis*. LH1 subunits (red) form a closed ellipse of 16 αβ-heterodynes around the RC subunits (purple) toped by the tetraheme cytochrome (green). Associated pigments are in yellow. For clarity, protein side chains are not shown.

ellipticity of the LH1 assembly (see below), the overall shape of the complex is roundish and consequently the complexes arrange in a pseudo-crystalline hexagonal closest packing, obviously due to the absence of LH2s which would have intercalated the core complexes. In such an arrangement, all core complexes are structurally identical and their molecular neighbourhoods are identical (Fig. 9c). As a consequence, all RCs are functionally equal and the chance that a RC is occupied by the primary photoreaction is equal for all complexes.

Using the AFM tip as a nanodissector [32,34], the strongly protruding 4Hcyt can be removed and a RC $(L,M,H)_{(1)}$–$LH1(\alpha,\beta)_{(16)}$ remains (Fig. 9a and b2). The topography reveals that, in all individual RC $(L,M,H)_{(1)}$–$LH1(\alpha,\beta)_{(16)}$ complexes, the surfaces of the L and M subunits of the RC are located on one side of the LH1 ring. The RC adopts preferred orientation suggesting specific interactions between the RC and LH1 subunits rather than a continuum of possible orientations within the antenna ring interaction. Another important feature of the AFM topographs is that the LH1 subunit distribution is found to be elliptical with length differences of the long and the short axis of about 10%. The orientation of the long axis of the LH1 $(\alpha,\beta)_{(16)}$ ellipsis coincides with the long axis of the RC $(L,M,H)_{(1)}$ topography. The ellipticity of the LH1 with an associated RC reflects a strong and specific interaction between the components of the core complex.

LH1 $(\alpha,\beta)_{(16)}$ rings, where the $4Hcyt_{(1)}$–RC $(L,M,H)_{(1)}$ proteins have been removed, have also been imaged. They form a closed circle with ~100 Å top diameter consisting of 16 (α,β) subunits (Fig. 9a and b3). The subunits show a left-handed twist to the circle outside with lower peripheral than inner protrusions. The ellipticity of the LH1 $(\alpha,\beta)_{(16)}$ in complex with the RC $(L,M,H)_{(1)}$, compared to a circular LH1 $(\alpha,\beta)_{(16)}$ after removal of the RC, $(L,M,H)_{(1)}$ reflects a flexibility of the LH1 $(\alpha,\beta)_{(16)}$ assembly. Such flexibility and/or fluctuations of ellipticity of the LH1 ring has been proposed to favour the quinone/quinol passage through a closed LH1 $(\alpha,\beta)_{(16)}$ fence.

At this point, it has to be stressed that the *Blc. viridis* core complexes investigated in this work were never solubilised nor removed from the lipid bilayer and that no restrictions of crystallinity are applied to the LH1 architecture and the RC in the ring inside. This is important when comparing these data on the core complex of *Blc. viridis* in its native environment with those reported on the core complex of *R. rubrum* after purification and reconstitution in different 2D crystal forms (see above 4.1) [66,71].

### 4.2.3. The PSU of Rhodospirillum photometricum

The photosynthetic apparatus of *Rhodospirillum (Rsp.) photometricum*, a purple photosynthetic bacterium closely related to the better-known species *Rsp. rubrum*, is associated with stacked disk-like vesicles of intracytoplasmic membranes large enough for AFM analysis [44,45]. However, the purified large membrane vesicles did not collapse on the mica support and the upper membrane layer could not be imaged at high resolution because of weak attachment. To alleviate this problem, the upper membrane layer was removed by nanodissection with the AFM tip. This protocol allowed to obtain high-resolution topographs of the firmly attached lower bilayer exposing the periplasmic membrane surface. LH2 complexes and monomeric core complexes (RC $(L,M,H)_{(1)}$–LH1 $(\alpha,\beta)_{(16)}$) have been analysed at 12 Å and 15 Å resolution, respectively (Fig. 10a) [44,45].

The majority of the LH2 complexes were aligned and averaged to give a ring shaped assembly with 9-fold symmetry. On closer examination of the raw data images, it was obvious that LH2s of various sizes were present within the native membranes. Separation of the particles using neuronal network classification of their rotational power spectrum revealed for the first time a heterogeneity of

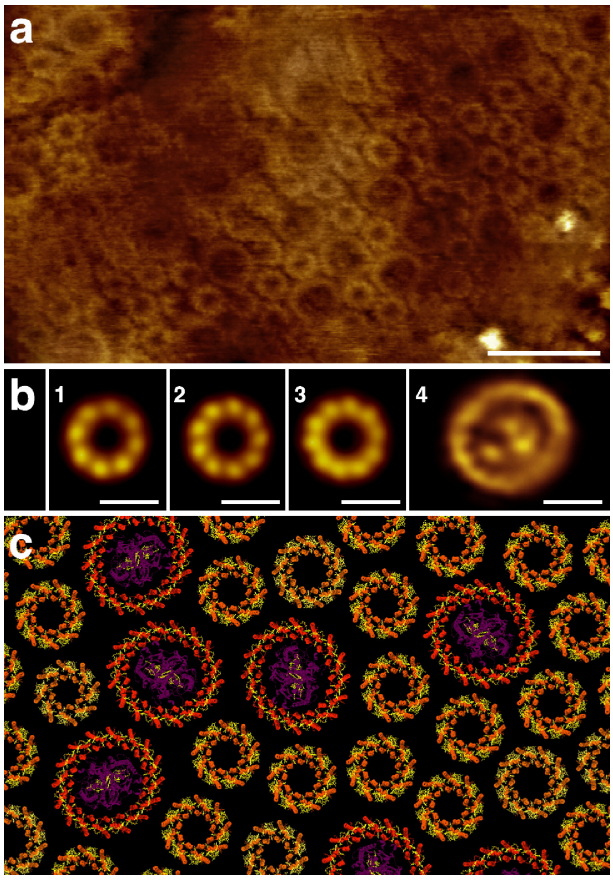


Fig. 10. AFM Images of the native membrane of *Rhodospirillum photometricum*. High-resolution AFM analysis of the native photosynthetic membrane of *Rsp. photometricum* (adapted from [44, 45]). (a) Raw data AFM topograph revealing the complex mixture of LH2 and core complexes in the native photosynthetic membrane of *Rsp. Photometricum* (scale bar: 20 nm). (b) Averages of the LH2 complexes with variable size. (1) LH2$(\alpha,\beta)_{(8)}$; (2) LH2$(\alpha,\beta)_{(9)}$; (3) LH1$(\alpha,\beta)_{(10)}$. The majority (~70%) of the LH2 rings are nonameric. Rarely, larger 'empty rings with diameters up to ~80 Å were found. (4) The core complex comprises a closed ellipse of LH1 surrounding one RC with a RC $(L,M,H)_{(1)}$–LH1$(\alpha,\beta)_{(16)}$ stoichiometry (scale bar: 5 nm). (c) Model of the complex assembly in the native membrane of *Rsp. photometricum*. LH2 subunits (orange) arrange in variable sized rings (8 mers, 9 mers, or 10 mers) intercalating the core complexes consisting of LH1 subunits (red) forming a closed ellipse of 16 α,β-heterodimers around the RC subunits (purple). Associated pigments are in yellow. For clarity, protein side chains are not shown.

the LH2 complex stoichiometry: 70% of the complexes were nonameric (Fig. 10b2), while 30% of the complexes had either significantly smaller or larger diameters, corresponding to 8- (Fig. 10b1) or to 10-fold symmetry (Fig. 10b3). Since the images were acquired on native membranes, the heterogeneity found represents an inherent feature of native LH2 assembly in *Rsp. photometricum*. At a molecular level, such variability in the ring size can be reached through small changes in the interaction angle between adjacent subunits.

In contrast to the heterogeneity found for LH2 complexes, the LH1–RC assemblies of the core complexes appeared uniform in size. The core complexes were monomeric with a closed LH1 assembly around the RC. The LH1 assembly of the core complex formed a closed ellipse with long and short axes of 95 Å and 85 Å, respectively (Fig. 10b4). The general closed architecture of the elliptical core complex of *Rsp. photometricum* is similar to that reported for *Rsp. rubrum* [66] and *Blc. viridis* [30] but different from the dimeric "open" core complexes of *Rb. sphaeroides* [68] and *Rb. blasticus* [43] (see below, Section 4.2.4).

Besides the major technical advance represented by the acquisition of such highly resolved data on a complex membrane, the images gave novel insights into the assembly of the PSU in the membranes of *Rsp. photometricum* (Fig. 10c). Analysis of the distribution of the complexes showed that their arrangement is far from random with significant clustering both of antenna complexes and core complexes. Within the membrane, smooth and corrugated patches are observed, indicating that the membrane parts containing the PSU proteins are connected to protein-free lipid bilayers [44]. This important observation demonstrates that all membrane proteins of the photosynthetic apparatus have a tendency to cluster together and that the generated structure is due to specific protein–protein interactions and not exclusively to the high protein concentration and packing difficulties. From a functional point of view, this observation seems reasonable and not very surprising as each light-harvesting component that segregates away from the system is non-functional, since it cannot pass its energy to a neighbouring complex and eventually to the RC.

Surprisingly, there is no fixed PSU structure as proposed in numerous models of the PSU [48,111,112]. Although the membranes contain in average 5 LH2s per core, cores making multiple contacts were found. Theoretically, the molecules could arrange in a manner avoiding any core–core contacts. This is not the case and only 27% of all core complexes were found completely surrounded by LH2 rings. Significantly, 73% of the core complexes make 1, 2 or maximally 3 core–core contacts. This means that, in a membrane where protein-free bilayer could be occupied, the core–core clustering must have a functional significance. This observation is important because it has already been suggested by functional studies in different organisms that the RCs are grouped together to explain their efficiency and saturation behaviour. Functionally, it would increase the possibility of an excitation being trapped by an RC under conditions where the rate of electron transport and photon capture are approximately balanced. Under these circumstances, an excitation as it diffuses through the antenna system will find, with a reasonable probability, a first RC that is already occupied in performing the initial photochemical reactions.

### *4.2.4. The PSU of Rhodobacter blasticus*

The structural analysis of *Rhodobacter* core complexes is of particular interest since it is the only family in which a small transmembrane protein, named PufX, has been

identified crucial for bacterial growth under anaerobic photosynthetic conditions and for the fast exchange of quinones between the RC and the cyt *bc1* complex [122–124]. Low resolution (20 Å–30 Å) negative stain projection maps of native crystalline tubular membranes of LH2-deleted *Rb. sphaeroides* have revealed dimeric core complexes with S-shaped LH1 assemblies housing the two RCs [61,125]. In both negative stain maps, the LH1 assembly of each core covered ~3/4 of a full ellipse, corresponding to 12±1 LH1 αβ heterodimers per core. Structural studies of 2D crystals of RC–LH1–PufX core complexes purified from *Rb. sphaeroides* have also been performed. First, a cryo-EM projection map, revealing the transmembrane protein portions, showed an S-shaped core complex dimer with a ~30 Å wide protein-free gap in each LH1 assembly [68]. A maximum density was found at the dimer junction, leading the authors to propose a localization of the two PufX proteins at the dimer junction. Second, a negative stain EM projection map showed monomeric core complexes with closed LH1–PufX rings [125]. The discrepancies between the two studies are most probably due to different sample preparations, i.e., solubilisation, purification and reconstitution. To avoid preparation artifacts and to unambiguously localize the different subunits of *Rhodobacter* core complexes, the acquisition of data at molecular resolution under close to native conditions was required.

Membranes of wild type *Rb. blasticus*, a closely related strain to the well-studied *Rb. sphaeroides*, have been imaged at high resolution by AFM [43]. The purified native photosynthetic membrane are uniformly small sized vesicles with a diameter of ~50 nm. In order to make these membranes amenable to AFM analysis, the small vesicles were fused by freeze-thaw cycles. This led to the formation of vesicular membranes with sizes up to 1 μm which, although not completely flat, were amenable to high-resolution topographs. Due to the 'mechanics' of this fusion process, AFM topographs revealed a mixture of proteins in 'up and down' orientations as evidenced by the presence of two types of complexes protruding differently from the membrane. Topographs could be acquired at 15 Å resolution and revealed both periplasmic and cytoplasmic surfaces of LH2 complexes and of dimeric core complexes (Fig. 11a) [43].

The LH2 complexes are nonameric rings inserted with their 9-fold axis perpendicular to the membrane. They protruded 6 Å on the cytoplasmic (Fig. 11b1) and 17Å on the periplasmic side (Fig. 11b2). Importantly, high-resolution topographs of PufX-containing core complexes have been acquired by taking advantage of their 'up and down' orientation (Fig. 11b3 and b4) that allows high resolution imaging of the periplasmic surface devoid of the strongly protruding H-subunit of the RC (Fig. 11b4). AFM topographs reveal that core complexes assemble in S-shaped dimeric complexes of ~10 nm × ~20 nm size. Each core complex is composed of a clearly open LH1 assembly with a gap of ~25 Å width, housing one reaction centre. Furthermore, the LH1 assembly of each core is elliptical

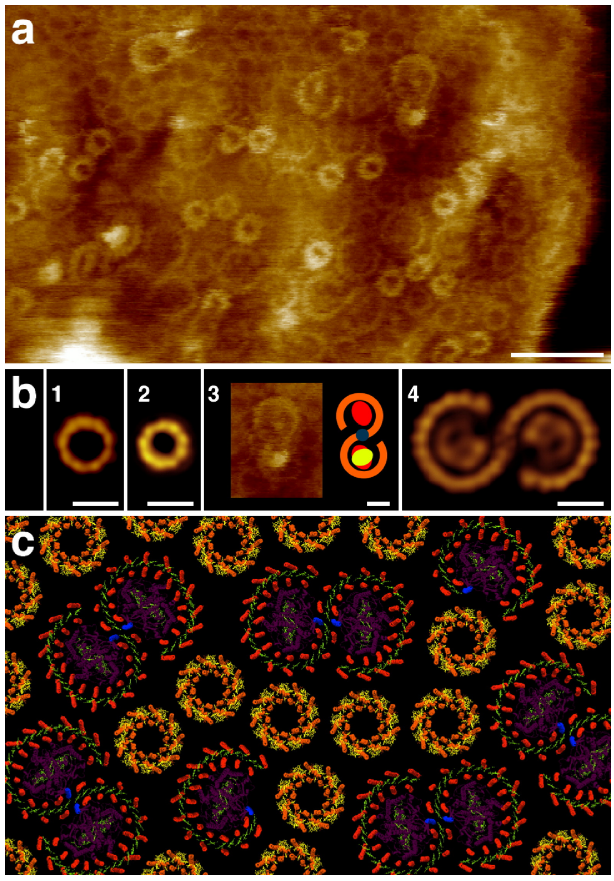


Fig. 11. AFM Images of the native membrane of *Rhodobacter blasticus*. High resolution AFM analysis of the native photosynthetic membrane of *Rb. blasticus* (adapted from [43]). (a) Raw data AFM topograph revealing the complex mixture of LH2 and core complexes in the fused native photosynthetic membranes of *Rb. blasticus*. The PufX containing core complexes form stable dimers (~75%) with a stoichiometry of $(LH1(\alpha,\beta)_{(13)}–RC_{(1)}–PufX_{(1)})_2$. A smaller fraction (~25%) are monomeric $LH1(\alpha,\beta)_{(13)}–RC_{(1)}–PufX_{(1)}$ complexes. Scale bar: 20 nm. (b) Due to the fusion of the native membranes, both surfaces of LH2s and core complexes could be analysed. (1) cytoplasmic surface of $LH2(\alpha,\beta)_{(9)}$ with a top ring diameter of 55 Å and protrusion height of 6 Å; (2) periplasmic surface of LH2 $(\alpha,\beta)_{(9)}$ with a top ring diameter of 45 Å and protrusion height of 17 Å; (3) cytoplasmic view of a core complex dimer (the H-subunit has been removed by the AFM tip from the top RC (as indicated by the sketch); (4) 2-fold symmetrised average of the periplasmic surface of the $(LH1(\alpha,\beta)_{(13)}–RC_{(1)}–PufX_{(1)})_2$ core complex. Scale bar: 5 nm. (c) Model of the complex assembly in the native membrane of *Rb. blasticus*. LH2 subunits (orange) 9 mers intercalating dimeric (75%) and monomeric (25%) core complexes consisting of S-shaped LH1 assemblies (red) around two RCs (purple). At the core complex dimer centre, two PufX subunits (blue) hold the two core complexes together. Associated pigments are in yellow. For clarity, protein side chains are not shown.

with long and short axes of 100 Å and 90 Å, respectively. The ellipticity of the core complexes of *Rb. Blasticus* is particularly astonishing since one would expect larger flexibility of an open LH1 assembly. It is thus likely that the ellipticity results from specific interactions over large parts of the RC. AFM topographs also revealed particular features of the LH1 assembly at the dimer centre: an enlarged and depressed topography in which two tiny protrusions are visible. Since the LH1 assembly is com-

posed of multiple identical αβ heterodimers and one PufX polypeptide [124], the particular topography at the dimer centre was attributed to the two PufX peptides from the two cores holding the dimer together. This assignment was in agreement with previous EM studies of dimeric core complexes of *Rb. sphaeroides* in native crystalline tubes and in 2D crystals of purified proteins [61,68]. Based on these data, a structural model was proposed for the subunit organisation of the *Rhodobacter* core complex (Fig. 11c). The core complex is an S-shaped dimer composed of 2 RCs. Each RC is encircled by an open ellipse composed of 13 LH1 αβ-heterodimers. At the dimer centre, two PufX subunits, one of each core, are identified. This model provides explanation for the PufX-induced dimerisation of the *Rhodobacter* core complex which indirectly favours quinol/quinone passage [43].

Although the 'up and down' membrane fusion process impeded a detailed analysis of the position and association of the different photosynthetic complexes in the native membrane, regions corresponding to one orientation showed that the complexes are in physical contact with neighbouring complexes (Fig. 11c). The distances between the LH2s are similar to LH2–LH2 distances found in 2D-crystals with a hexagonal lattice. In addition, many LH2 rings are in direct contact with the PufX-containing core complexes facilitating the transfer of excitation energy from LH2 to LH1 and hence to the RC. Such physical contact between the different complexes, also reported by AFM in other native membranes, would represent the basic requirement for the efficient harvesting, transmission and trapping of light energy in photosynthetic bacteria.

#### *4.2.5. The PSU of Rhodobacter sphaeroides*

AFM analysis of membrane patches of intracytoplasmic membrane vesicles from *Rb. sphaeroides* have revealed the arrangement of the photosynthetic complexes in this most studied photosynthetic bacterium [46]. After isolation, the membranes were treated with sub-solubilising amounts of detergent and the large, probably fused, membrane fragments analyzed by AFM. Two types of complexes could be visualised: large circular complexes with protruding central protein, corresponding to core complexes, and smaller rings of about 7 nm in diameter with no central density, corresponding to LH2 complexes (Fig. 12a) [46].

Although the resolution was not sufficient to analyse the precise stoichiometry of the LH2 complexes, most of them seemed to be composed of nine subunits, consistent with previous structural data on this light-harvesting complex [18,62]. Some but not all LH2s appeared to be slightly tilted 3–4° from the vertical. This tilt was not confined to LH2s and close inspection of few LH1s revealed also an average 4.8° tilt. It is not clear whether the tilting of LH2 and LH1 complexes has any functional significance but the mutual inward tilt of the RC–LH–PufX complexes indicates that it may be a consequence of the dimerisation process.

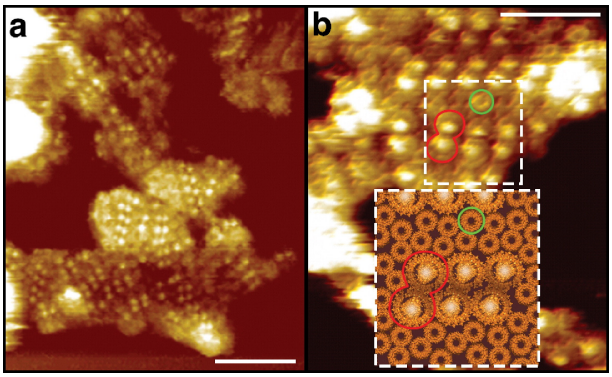


Fig. 12. AFM images of the native membrane of *Rhodobacter sphaeroides*. High-resolution AFM analysis of the native photosynthetic membrane of *Rb. sphaeroides* (adapted from [46]). (a) Large-scale view of several fragments of fused native photosynthetic membranes of *Rb. sphaeroides* (Scale bar: 100 nm). (b) Higher magnification AFM topograph. The inset is a representation of the region denoted by the dashed box in the centre, using model structures derived from atomic resolution data. A typical RC–LH1–PufX dimer is delineated in both images by a red outline and a representative LH2 complex by a green circle. Scale bar: 50 nm.

The larger features in the AFM topographs are LH1–RC–PufX core complexes of about 12 nm in diameter. They comprise an LH1 ring surrounding a central bright region about 4 nm above the lipid bilayer, which corresponds to the H subunit of the RC complex. These RC–LH1–PufX complexes are usually dimeric and the dimers are arranged in rows up to 6 dimers (Fig. 12b). From such an organisation, it becomes clear why mutants lacking LH2 form tubular membranes containing linear rows of dimers aligned in parallel. This is a natural consequence of removing the LH2 complexes that normally separate rows of dimers. Unfortunately, due to a tilt of the LH1–RC–PufX complexes, the central part of each dimer could not be analysed in details, preventing the identification of the PufX polypeptide as well as the completeness of the LH1 ring. Whatever, a model of the LH1–RC–PufX dimers has been formulated (inset in Fig. 12b) by arranging the structural information available from a negative stain EM projection map of LH1–RC–PufX 2D crystals [125].

The AFM topographs gave a precise view of the relative positions and associations of the photosynthetic complexes in their native environment. Two types of organisation were found for the peripheral light harvesting LH2 complexes: in the first, groups of 10–20 LH2s molecules interconnected the linear arrays of RC–LH1–PufX dimers; in the second, LH2 complexes were found outside these regions in larger clusters. In addition to making contact with each other, some of the LH2 rings are found in close physical association with the core complexes. There is physical continuity between individual LH2 complexes and between LH2 and core dimers, facilitating the transfer of excitation energy from LH2 to LH1 and hence to the RC. It is possible that the linear arrays of LH–RC–PufX complexes cooperate in the overall process of energy trapping because, if any RC is already undertaking photochemical charge

separation and thus available for receiving excitation energy from its LH1 ring, the LH1 excitation can migrate along a succession of such dimers until an "open" RC is reached (see also [126]).

Another interesting observation was the use of AFM to evidence a low lateral mobility of the different complexes as shown by a sequence of 10 consecutive images obtained from the same membrane patch [46]. Although an interaction with the mica support could account for this very low lateral mobility, it is tempting to suggest that the close packing of the complexes within the native membranes probably prevents the lateral diffusion of individual components.

### 4.3. Current views of the photosynthetic apparatus by AFM

Here, we have reviewed all the recent AFM reports performed on the individual components of the photosynthetic apparatus and on native bacterial photosynthetic membranes. These data allow completing the picture of the organisation of the antenna complexes and the RCs, giving novel insights into the basic requirement for the efficient harvesting, transmission and trapping of light energy in these bacteria.

It is clearly shown in all the bacterial photosynthetic membranes analysed (*Blc. viridis* [30], *Rsp. photometricum* [44,45], *Rb. blasticus* [43] and *Rb. sphaeroides* [46]) that the photosynthetic complexes are densely packed within the native membranes. There is physical continuity between individual LH2 complexes and between LH2 and core complexes facilitating the transfer of excitation energy from LH2 to LH1 and hence to the RC. Interestingly, in *Rsp. photometricum* membranes, the coexistence of pure lipids and PSU-dense domains could be visualised. This observation demonstrates that, although the photosynthetic proteins have enough membrane space to dilute into, they have a tendency to cluster together and that the generated structure is due to specific protein–protein interactions and not exclusively to the high protein concentration and packing difficulties. From a functional point of view, the close packing arrangement of light harvesting complexes visualised by AFM is not surprising as each light-harvesting component that segregates away from the system is non-functional, i.e., its excitation energy after photon trapping will be lost since it cannot pass its energy to a neighbouring complex and eventually to the RC.

Another important observation deduced from the in situ AFM topographs of different photosynthetic bacteria is that there is no fixed PSU structure. Different LH2–core complexes organisations have been visualised. These organisations vary from one species to the other and also importantly within one species. These direct images of intact photosynthetic membranes can be compared with the numerous models of a bacterial photosystem that have been proposed to explain its enormous efficiency [48,111,112]. In particular, the often-proposed model of a photosynthetic unit consisting of a core complex completely surrounded by LH2s has been in fact scarcely observed. In *Rsp. photometricum* as well as in *Rb. sphaeroides*, although the membranes contain enough LH2 complexes, large LH2-enriched domains and cores making multiple contacts have been visualised in spite of finding separated cores completely surrounded by LH2. The AFM observations of multiple core–core interactions in *Rsp. photometricum* as well as the linear arrays of LH–RC–PufX complexes in *Rb sphaeroides* mean that the core–core clustering must have a functional significance and cooperate in the overall process of energy trapping. In situations when light is not limiting, it becomes probable that if any RC is already undertaking photochemical charge separation and thus not available for receiving excitation energy from its LH1 ring, the LH1 excitation can migrate along a succession of core complexes until a free RC available for photochemistry is reached.

However, such a close packing of photosynthetic complexes raises a problem to all processes which need free diffusion within the membrane, such as the quinone/quinol transfer between the RC and the cyt *bc1* complex. The migration of Q/QH2 is strongly debated in light of the LH1 architecture around the RC, whether the LH1 assembly is closed or open. This is still an interesting point, but regarding a membrane in which the protein components are kept in physical protein–protein contact over several hundreds of square nanometres, the problem of Q/QH2 passage becomes a more general problem since no cyt *bc1* is found in close proximity to the RCs (see below). How is it possible to have protein–protein contacts demanded by the functionality of the PSU within a membrane and still allow efficient Q/QH2 diffusion within this membrane? The transfer of redox energy between the RC and cyt *bc1* is thus difficult to understand in light of the PSU structure observed by AFM in native photosynthetic membranes: it is unclear how quinones can escape from the RC, cross the LH1 fence and then diffuse through a densely packed membrane to find a relatively distant cyt *bc1*. Might there exist specific channels for diffusion or chains of quinones to facilitate this process? First indications about large quinone pools come from exogenous cytochrome c2 oxidation measurements, indicating more than 10 quinones associated to each RC [127–129].

An intriguing 'negative' result of the AFM studies is the complete absence of the cyt *bc1* complex in all the membranes imaged from *Blc. viridis*, *Rsp. photometricum*, *Rb. blasticus* and *Rb. sphaeroides*. In view of the high resolution imaging, the cyt *bc1* complexes, which are qualitatively found in SDS-PAGE analysis of the membrane preparations, should be easily recognizable by AFM as relatively large dimeric molecules with an overall size of ~5 nm × ~10 nm perpendicular to the membrane plane. It seems unrealistic to presume that all the cyt *bc1* complexes have selectively segregated away from their initial native positions while all the RCs, LH1s and LH2s have remained in a complex mixture. It can be suggested that, in cells, the

cyt *bc1* complex is located close to the cytoplasmic membrane or on the edges of the intracytoplasmic invaginations and that the flat surfaces of the intracytoplasmic invaginations imaged by AFM contain the PSU proteins at high density and very little, if any, cyt *bc1*. It is also possible that the PSU-dense intracytoplasmic membranes adsorb preferentially to the AFM support. However, all possible explanations implicate a location of the cyt *bc1* complex far from many of the RCs. This finding is in obvious contradiction with the functional coupling between the RCs and the cyt *bc1* complexes and, even more, with the notion of functional supercomplexes comprising core-complexes and cyt *bc1* complexes [130–132].

## 5. Conclusion

Exploration of the machinery involved in the conversion of light energy into chemical energy can be understood because the purple photosynthetic bacteria offer a unique system for obtaining and integrating structural and functional information. This system has been paradigm for testing the usefulness of AFM to analyse at high resolution an assembly of multi-component membrane protein complexes. In this review, we have compiled all the recent data that definitely demonstrate that AFM is a unique tool to investigate in situ multi-protein complexes at molecular resolution. The molecular organisation of photosynthetic complexes have been studied at high resolution in native membranes without the need of solubilisation, purification and crystallisation steps. The images now being produced are spectacular and the way is clear to use this technology to map antenna organisation within intact photosynthetic membranes. It is to be expected over the next few years that many publications will be presented in this area and will hopefully answer many of the remaining questions concerning purple bacterial photosynthesis. For example, further questions can now be addressed by AFM: how these multiprotein systems evolve and how do they compare between species to fulfil their physiological function? How does the level of LH2 in low light grown cells affect the architecture? Where are the cyt *bc1* and the F0F1 ATPases localised? Are supramolecular complexes between core complexes and cyt *bc1* present? In addition, using the AFM stylus as a nanotool that allows single molecules to be manipulated, supramolecular structures and single biomolecules can be dissected and forces measured. Such experiments will give novel information on the nature of molecular interactions and the forces that stabilize the building blocks.

Finally, the data demonstrate that the AFM will become a key technique for the investigation of integrated photosynthetic apparatus ranging from bacteria to plants but also of protein assemblies in native membranes in general. Indeed, the organisation of the intact machinery in biological membranes represents a major challenge in structural biology. In the future, the ability of AFM to image more complexes biological systems will deliver novel insights into the biogenesis of various native membranes, into the interactions between similar or different membrane proteins within a membrane and into the formation of supramolecular complexes. It will be a challenge to analyse by AFM the energy transducing machinery in the respiration process, to understand the assembly of membrane proteins into rafts and to investigate some processes involved in trafficking and signal transduction.

## Acknowledgements

We are grateful to B. Robert, J. Seguin, J.N. Sturgis, V. Prima, A. Vermeglio and P. Joliot for collaborative work and fruitful discussions. We also thank N. Hunter for providing (Figs. 7, 8 and 12). This study was supported by the Institut Curie, the CNRS, the INSERM (to S. S.), a grant 'ACI NanoSciences 2004' (NR 206) and a grant from the European Community (HPRN-CT-2002-00269).

## References

[1] W. Kühlbrandt, E. Gouaux, Membrane proteins, Curr. Opin. Struct. Biol. 9 (1999) 445–447.
[2] G. Binnig, C.F. Quate, C. Gerber, Atomic force microscope, Phys. Rev. Lett. 56 (1986) 930–933.
[3] A. Engel, H. Gaub, D.J. Müller, Atomic force microscope: a forceful way with single molecules, Curr. Biol. 9 (1999) 133–136.
[4] A. Engel, D.J. Müller, Observing single biomolecules at work with the atomic force microscope, Nat. Struct. Biol. 7 (2000) 715–718.
[5] M. Bezanilla, C.J. Bustamante, H.G. Hansma, Improved visualization of DNA in aqueous buffer with the atomic force microscope, Scanning Microsc. 7 (1993) 1145–1148.
[6] D.J. Müller, F.A. Schabert, G. Büldt, A. Engel, Imaging purple membranes in aqueous solutions at subnanometer resolution by atomic force microscopy, Biophys. J. 68 (1995) 1681–1686.
[7] M. Fritz, M. Radmacher, J.P. Cleveland, M.W. Allersma, R.J. Steward, R. Gieselmann, P. Janmey, C.F. Schmidt, P.K. Hansma, Imaging globular and filamentous proteins in physiological buffer solutions with tapping mode atomic force microscopy, Langmuir 11 (1995) 3529–3535.
[8] D.J. Müller, A. Engel, The height of biomolecules measured with the atomic force microscope depends on electrostatic interactions, Biophys. J. 73 (1997) 1633–1644.
[9] C. Legrimellec, E. Lesniewska, M.C. Giocondi, C. Cachia, J.P. Schreiber, J.P. Goudonnet, Imaging of the cytoplasmic leaflet of the plasma membrane by atomic force microscopy, Scanning Microsc. 9 (1995) 401–411.
[10] H.G. Hansma, D.E. Laney, M. Bezanilla, R.L. Sinsheimer, P.K. Hansma, Applications for atomic force microscopy of DNA, Biophys. J. 68 (1995) 1672–1677.
[11] D.M. Czajkowsky, Z. Shao, Submolecular resolution of single macromolecules with atomic force microscopy, FEBS Lett. 430 (1998) 51–54.
[12] H.G. Hansma, J. Hoh, Biomolecular imaging with the atomic force microscope, Annu. Rev. Biomol. Struct. 23 (1994) 115–139.
[13] J. Mou, D.M. Czajkowsky, S. Sheng, R. Ho, Z. Shao, High resolution surface structure of *E. coli* GroES oligomer by atomic force microscopy, FEBS Lett. 381 (1996) 161–164.

[14] M. Radmacher, R.W. Tillamnn, M. Fritz, H.E. Gaub, From molecules to cells: imaging soft samples with the atomic force microscope, Science 257 (1992) 1900–1905.
[15] Z.F. Shao, J. Yang, Progress in high resolution atomic force microscopy in biology, Q. Rev. Biophys. 28 (1995) 195–251.
[16] Z.F. Shao, J. Yang, A.P. Somlyo, Biological atomic force microscopy: from microns to nanometers and beyond, Annu. Rev. Cell Dev. Biol. 11 (1995) 241–265.
[17] D.J. Müller, J.B. Heymann, F. Oesterhelt, C. Moller, H. Gaub, G. Büldt, A. Engel, Atomic force microscopy of native purple membrane, Biochim. Biophys. Acta 1460 (2000) 27–38.
[18] S. Scheuring, J. Seguin, S. Marco, D. Lévy, C. Breyton, B. Robert, J.-L. Rigaud, AFM characterization of tilt and intrinsic flexibility of *Rhodobacter sphaeroides* light harvesting complex 2 (LH2), J. Mol. Biol. 325 (2003) 569–580.
[19] S. Scheuring, P. Ringler, M. Borgina, H. Stahlberg, D.J. Müller, P. Agre, A. Engel, High resolution topographs of the *Escherichia coli* waterchannel aquaporin Z, EMBO J. 18 (1999) 4981–4987.
[20] S. Scheuring, F. Reiss-Husson, A. Engel, J.-L. Rigaud, J.-L. Ranck, High resolution topographs of the *Rubrivivax gelatinosus* light-harvesting complex 2, EMBO J. 20 (2001) 3029–3035.
[21] D. Fotiadis, L. Hasler, D.J. Müller, H. Stahlberg, J. Kistler, A. Engel, Surface tongue- and-groove contours on lens MIP facilitate cell-to-cell adherence, J. Mol. Biol. 300 (2000) 779–789.
[22] H. Stahlberg, D.J. Müller, K. Suda, D. Fotiadis, A. Engel, U. Matthey, T. Meier, P. Dimroth, Bacterial ATP synthase has an undacemeric rotor, EMBO Rep. 2 (2001) 229–235.
[23] S. Scheuring, D. Fotiadis, C. Möller, S.A. Müller, A. Engel, D.J. Müller, Single proteins observed by atomic force microscopy, Single Mol. 2 (2001) 59–67.
[24] D.J. Müller, A. Engel, U. Matthey, T. Meier, P. Dimroth, K. Suda, Observing membrane protein diffusion at subnanometer resolution, J. Mol. Biol. 327 (2003) 925–930.
[25] J. Mou, S. Sheng, R. Ho, Z. Shao, Chaperonins GroEL and GroES: views from atomic fore microscopy, Biophys. J. 71 (1996) 2213–2221.
[26] J.X. Mou, J. Yang, Z.F. Shao, Atomic force microscopy of cholera toxin B-oligomers bound to bilayers of biologically relevant lipids, J. Mol. Biol. 248 (1995) 507–512.
[27] D.J. Müller, D. Fotiadis, A. Engel, Mapping flexible protein domains at subnanometer resolution with the AFM, FEBS Lett. 430 (1998) 105–111.
[28] C. Goldsbury, J. Kistler, U. Aebi, T. Arvinte, G.J.S. Cooper, Watching amyloid fibrils grow by time-lapse atomic force microscopy, J. Mol. Biol. 285 (1999) 33–39.
[29] D. Stoffler, K.N. Goldie, B. Feja, U. Aebi, Calcium-mediated structural changes of native nuclear pore complexes monitored by time-lapse atomic force microscopy, J. Mol. Biol. 287 (1999) 741–752.
[30] S. Scheuring, J. Seguin, S. Marco, D. Lévy, B. Robert, J.L. Rigaud, Nanodissection and high-resolution imaging of the *Rhodopseudomonas viridis* photosynthetic core-complex in native membranes by AFM, Proc. Natl. Acad. Sci. U. S. A. 100 (2003) 1690–1693.
[31] I. Reviakine, W. Bergsma-Schutter, A. Brisson, Growth of protein 2-D crystals on supported planar lipid bilayers imaged in situ by AFM, J. Struct. Biol. 121 (1998) 356–361.
[32] J.H. Hoh, R. Lal, S.A. John, J.-P. Revel, M.F. Arnsdorf, Atomic force microscopy and dissection of gap junctions, Science 253 (1991) 1405–1408.
[33] D. Fotiadis, D.J. Müller, G. Tsiotis, L. Hasler, P. Tittmann, T. Mini, P. Jenö, H. Gross, A. Engel, Surface analysis of the photosystem I complex by electron and atomic force microscopy, J. Mol. Biol. 283 (1998) 83–94.
[34] D. Fotiadis, S. Scheuring, S.A. Müller, A. Engel, D.J. Müller, Imaging and manipulation of biological structures with the AFM, Micron 33 (2002) 385–397.
[35] F.A. Schabert, C. Henn, A. Engel, Native *Escherichia coli* OmpF porin surfaces probed by atomic force microscopy, Science 268 (1995) 92–94.
[36] S. Scheuring, H. Stahlberg, M. Chami, C. Houssin, J. Rigaud, A. Engel, Charting and unzipping the surface-layer of *Corynebacterium glutamicum* with the atomic force microscope, Mol. Microbiol. 44 (2002) 675–684.
[37] E.-L. Florin, V.T. Moy, H.E. Gaub, Adhesion forces between individual ligand-receptor pairs, Science 264 (1994) 415–417.
[38] V.T. Moy, E.-L. Florin, H.E. Gaub, Intermolecular forces and energies between ligands and receptors, Science 266 (1994) 257–259.
[39] F. Oesterhelt, D. Oesterhelt, M. Pfeiffer, A. Engel, H.E. Gaub, D.J. Müller, Unfolding pathways of individual bacteriorhodopsins, Science 288 (2000) 143–146.
[40] M. Rief, M. Gautel, F. Oesterhelt, J.M. Fernandez, H.E. Gaub, Reversible unfolding of individual titin immunoglobulin domains by AFM, Science 276 (1997) 1109–1112.
[41] F.A. Schabert, A. Engel, Reproducible acquisition of *Escherichia coli* porin surface topographs by atomic force microscopy, Biophys. J. 67 (1994) 2394–2403.
[42] H. Seelert, A. Poetsch, N.A. Dencher, A. Engel, H. Stahlberg, D.J. Müller, Proton powered turbine of a plant motor, Nature 405 (2000) 418–419.
[43] S. Scheuring, J. Busselez, D. Levy, Structure of the dimeric PufX-containing core complex of *Rhodobacter blasticus* by in situ AFM, J. Biol. Chem. 180 (2005) 1426–1431.
[44] S. Scheuring, J.-L. Rigaud, J.N. Sturgis, Variable LH2 stoichiometry and core clustering in native membranes of *Rhodospirillum photometricum*, EMBO J. 23 (2004) 4127–4133.
[45] S. Scheuring, J.N. Sturgis, V. Prima, A. Bernadac, D. Lévy, J.-L. Rigaud, Watching the photosynthetic apparatus in native membranes, Proc. Natl. Acad. Sci. U. S. A. 101 (2004) 11293–11297.
[46] S. Bahatyrova, R.N. Frese, C.A. Siebert, J.D. Olsen, K.O. Van Der Werf, R. van Grondelle, R.A. Niederman, P.A. Bullough, C.N. Hunter, The native architecture of a photosynthetic membrane, Nature 430 (2004) 1058–1062.
[47] D. Fotiadis, Y. Liang, S. Filipek, D.A. Saperstein, A. Engel, K. Palczewski, Atomic-force microscopy: rhodopsin dimers in native disc membranes, Nature 421 (2003) 127–128.
[48] X. Hu, T. Ritz, A. Damjanovic, F. Autenrieth, K. Schulten, Photosynthetic apparatus of purple bacteria, Q. Rev. Biophys. 35 (2002) 1–62.
[49] R. van Grondelle, J.P. Decker, T. Gillbro, V. Sundstrom, Energy transfer and trapping in photosynthesis, Biochim. Biophys. Acta 1187 (1994) 1–65.
[50] M. Yang, R. Agarwal, G.R. Fleming, The mechanisms of energy transfer in photosynthetic purple bacteria, J. Photochem. Photobiol., A Chem. 142 (2001) 107–119.
[51] V. Sundström, T. Pullerits, R. van Grondelle, Photosynthetic light-harvesting: reconciling dynamics and structure of purple bacterial LH2 reveals function of photosynthetic unit, J. Phys. Chem., B 103 (1999) 2327–2346.
[52] J.P. Allen, G. Feher, T.O. Yeates, H. Komiya, D.C. Rees, Structure of the reaction center from *Rhodobacter sphaeroides* R-26: the protein subunits, Proc. Natl. Acad. Sci. U. S. A. 84 (1987) 6162–6166.
[53] J. Deisenhofer, O. Epp, K. Miki, R. Huber, H. Michel, Structure of the protein subunits in the photosynthetic reaction centre of *Rhodopseudomonas viridis* at 3 Å resolution, Nature 318 (1985) 618–624.
[54] G. Drews, Structure and function organization of light-harvesting complexes and photochemical reaction centers in membranes of phototrophic bacteria, Microbiol. Rev. 49 (1985) 59–70.
[55] J. Koepke, X. Hu, C. Muenke, K. Schulten, H. Michel, The crystal structure of the light-harvesting complex II (B800–850) from *Rhodospirillum molischianum*, Structure 4 (1996) 581–597.
[56] A.W. Roszak, T.D. Howard, J. Southall, A.T. Gardiner, C.J. Law,

N.W. Isaacs, R.J. Cogdell, Crystal structure of the RC–LH1 core complex from *Rhodopseudomonas palustris*, Science 302 (2003) 1969–1972.
[57] D. Xia, C.A. Yu, H. Kim, J.Z. Xia, A.M. Kachurin, L. Zhang, L. Yu, J. Deisenhofer, Crystal structure of the cytochrome bc1 complex from bovine heart mitochondria, Science 277 (1997) 60–66.
[58] G. McDermott, S.M. Prince, A.A. Freer, A.M. Hawthornthwaite-Lawless, M.Z. Papiz, R.J. Cogdell, N.W. Isaacs, Crystal structure of an integral membrane light-harvesting complex from photosynthetic bacteria, Nature 374 (1995) 517–521.
[59] M.Z. Papiz, S.M. Prince, T.D. Howard, R.J. Cogdell, N.W. Isaacs, The structure and thermal motion of the B800–850 LH2 complex from Rps.acidophila at 2.0 Å resolution and 100 K: new structural features and functionally relevant motions, J. Mol. Biol. 326 (2003) 1523–1538.
[60] S. Karrasch, P.A. Bullough, R. Ghosh, The 8.5 Å projection map of the light-harvesting complex I from *Rhodospirillum rubrum* reveals a ring composed of 16 subunits, EMBO J. 14 (1995) 631–638.
[61] C. Jungas, J.-L. Ranck, J.-L. Rigaud, P. Joliot, A. Vermeglio, Supramolecular organization of the photosynthetic apparatus of *Rhodobacter sphaeroides*, EMBO J. 18 (1999) 534–542.
[62] T. Walz, S.J. Jamieson, C.M. Bowers, P.A. Bullough, C.N. Hunter, Projection structures of three photosynthetic complexes from *Rhodobacter sphaeroides*: LH2 at 6 Å, LH1 and RC–LH1 at 25 Å, J. Mol. Biol. 282 (1998) 833–845.
[63] J. Ranck, T. Ruiz, G. Pehau-Arnaudet, B. Arnoux, F. Reiss-Husson, Two-dimensional structure of the native light-harvesting complex LH2 from *Rubrivivax gelatinosus* and of a truncated form, Biochim. Biophys. Acta 1506 (2001) 67–78.
[64] J.S. Jacob, K.R. Miller, Structure of a bacterial photosynthetic membrane, Arch. Biochem. Biophys. 223 (1983) 282–290.
[65] J.S. Jacob, K.R. Miller, Structure of a bacterial photosynthetic membrane: integrity of reaction centers following proteolysis and detergent solubilization, Biochem. Biophys. Res. Commun. 120 (1984) 164–171.
[66] S.J. Jamieson, P. Wang, P. Qian, J.Y. Kirkland, M.J. Conroy, C.N. Hunter, P.A. Bullough, Projection structure of the photosynthetic reaction centre-antenna complex of *Rhodospirillum rubrum* at 8.5 Å resolution, EMBO J. 21 (2002) 3927–3935.
[67] H. Engelhardt, A. Engel, W. Baumeister, Stoichiometric model of the photosynthetic unit of *Ectothiorhodospira halochloris*, Proc. Natl. Acad. Sci. U. S. A. 83 (1986) 8972–8976.
[68] S. Scheuring, F. Francia, J. Busselez, B. Melandri, J.-L. Rigaud, D. Lévy, Structural role of PufX in the dimerization of the photosynthetic core-complex of *Rhodobacter sphaeroides*, J. Biol. Chem. 279 (2004) 3620–3626.
[69] H. Stahlberg, J. Dubochet, H. Vogel, R. Ghosh, Are the light-harvesting I complexes from *Rhodospirillum rubrum* arranged around the reaction centre in a square geometry? J. Mol. Biol. 282 (1998) 819–831.
[70] A. Stamouli, S. Kafi, D.C. Klein, T.H. Oosterkamp, J.W. Frenken, R.J. Cogdell, T.J. Aartsma, The ring structure and organization of light harvesting 2 complexes in a reconstituted lipid bilayer, resolved by atomic force microscopy, Biophys. J. 84 (2003) 2483–2491.
[71] D. Fotiadis, P. Qian, A. Philippsen, P.A. Bullough, A. Engel, C.N. Hunter, Structural analysis of the reaction center light-harvesting complex I photosynthetic core complex of *Rhodospirillum rubrum* using atomic force microscopy, J. Biol. Chem. 279 (2004) 2063–2068.
[72] S. Bahatyrova, R.N. Frese, K.O. Van Der Werf, C. Otto, C.N. Hunter, J.D. Olsen, Flexibility and size heterogeneity of the LH1 light harvesting complex revealed by atomic force microscopy: functional significance for bacterial photosynthesis, J. Biol. Chem. 279 (2004) 21327–21333.
[73] R.P. Gonçalves, J. Busselez, D. Lévy, J. Seguin, S. Scheuring, Membrane insertion of *Rhodopseudomonas acidophila* light harvesting complex 2 (LH2) investigated by high resolution AFM, J. Struct. Biol. 149 (2005) 79–86.
[74] D.J. Müller, D. Fotiadis, S. Scheuring, S.A. Müller, A. Engel, Electrostatically balanced subnanometer imaging of biological specimens by atomic force microscopy, Biophys. J. 76 (1999) 1101–1111.
[75] D. Czajkowsky, M. Allen, V. Elings, Z. Shao, Direct visualization of surface charge in aqueous solution, Ultramicroscopy 74 (1998) 1–5.
[76] M. Fritz, M. Radmacher, M.W. Allersma, J.P. Cleveland, R.J. Stewart, P.K. Hansma, C.F. Schmidt, Imaging microtubules in buffer solution using tapping mode atomic force microscopy, SPIE 2384 (1995) 150–157.
[77] P.K. Hansma, J.P. Cleveland, M. Radmacher, D.A. Walters, P.E. Hillner, M. Bezanilla, M. Fritz, D. Vie, H.G. Hansma, C.B. Prater, J. Massie, L. Fukunaga, J. Gurley, V. Elings, Tapping mode atomic force microscopy in liquids, Appl. Phys. Lett. 64 (1994) 1738–1740.
[78] R. Hoper, T. Gesang, W. Possart, O.D. Hennemann, S. Boseck, Imaging elastic sample properties with an atomic force microscope operating in the tapping mode, Ultramicroscopy 60 (1995) 17–24.
[79] C. Möller, M. Allen, V. Elings, A. Engel, D.J. Müller, Tapping mode atomic force microscopy produces faithful high-resolution images of protein surfaces, Biophys. J. 77 (1999) 1050–1058.
[80] C.A.J. Putman, K.O. Vanderwerf, B.G. Degrooth, N.F. Vanhulst, J. Greve, Tapping mode atomic force microscopy in liquid, Appl. Phys. Lett. 64 (1994) 2454–2456.
[81] C.A.J. Putman, K.O. Vanderwerf, B.G. Degrooth, N.F. Vanhulst, J. Greve, Viscoelasticity of living cells allows high resolution imaging by tapping mode atomic force microscopy, Biophys. J. 67 (1994) 1749–1753.
[82] F.A. Schabert, J.P. Rabe, Vertical dimension of hydrated biological samples in tapping mode scanning force microscopy, Biophys. J. 70 (1996) 1514–1520.
[83] H.-J. Butt, Electrostatic interaction in atomic force microscopy, Biophys. J. 60 (1991) 777–785.
[84] H.-J. Butt, Electrostatic interaction in scanning probe microscopy when imaging in electrolyte solutions, Nanotechnology 3 (1992) 60–68.
[85] H.-J. Butt, M. Jaschke, W. Ducker, Measuring surface forces in aqueous solution with the atomic force microscope, Bioelect. Bioenerg. 38 (1995) 191–201.
[86] J. Israelachvili, Intermolecular and surface forces, second ed., Academic Press Limited, London, 1991.
[87] D.J. Müller, M. Amrein, A. Engel, Adsorption of biological molecules to a solid support for scanning probe microscopy, J. Struct. Biol. 119 (1997) 172–188.
[88] R.H. Alshakhshir, F.E. Regnier, J.L. White, S.L. Hem, Contribution of electrostatic and hydrophobic interactions to the adsorption of proteins by aluminium-containing adjuvants, Vaccine 13 (1995) 41–44.
[89] C.M. Roth, A.M. Lenhoff, Electrostatic and van der Waals contributions to protein adsorption: computation of equilibrium constants, Langmuir 9 (1993) 962–972.
[90] U.D. Schwarz, H. Haefke, P. Reimann, H.J. Guntherodt, Tip artefacts in scanning force microscopy, J. Microsc. (Oxford) 173 (1994) 183–197.
[91] J. Israelachvili, H. Wennerstrom, Role of hydration and water structure in biological and colloidal interactions, Nature 379 (1996) 219–225.
[92] G. Binnig, C. Gerber, E. Stoll, T.R. Albrecht, C.F. Quate, Atomic resolution with atomic force microscopy, Europhys. Lett. 3 (1987) 1281–1286.
[93] J. Frank, M. Radermacher, P. Penczek, J. Zhu, Y. Li, M. Ladjadj, A. Leith, SPIDER and WEB: processing and visualization of images in 3D electron microscopy and related fields, J. Struct. Biol. 116 (1996) 190–199.
[94] R. Marabini, I.M. Masegosa, C. San Martin, S. Marco, J.J. Fernandez, C.G. de la Fraga, J.M. Carazo, Xmipp: an image

processing package for electron microscopy, J. Struct. Biol. 116 (1996) 237–240.
[95] M. Unser, B.L. Trus, A.C. Steven, A new resolution criterion based on spectral signal-to-noise ratios, Ultramicroscopy 23 (1987) 39–52.
[96] M. Unser, B.L. Trus, J. Frank, A.L. Steven, The spectral signal-to-noise ration resolution criterion: computational efficiency and statistical precision, Ultramicroscopy 30 (1989) 429–434.
[97] N. Nelson, A. Ben-Shem, The complex architecture of oxygenic photosynthesis, Nat. Rev., Mol. Cell Biol. 5 (2004) 971–982.
[98] V. Sundstrom, R. van Grondelle, in: R.E. Blankenship, M.T. Madigan, C.E. Bauer (Eds.), Anoxygenic photosynthetic bacteria, Kluwer Academic Publishers, Netherlands, 1995, pp. 373–384.
[99] T. Polivka, V. Sundstrom, Ultrafast dynamics of carotenoid excited states—From solution to natural and artificial systems, Chem. Rev. 104 (2004) 2021–2072.
[100] R.J. Cogdell, A.T. Gardiner, A.W. Roszak, C.J. Law, J. Southall, N.W. Isaacs, Rings, ellipses and horseshoes: how purple bacteria harvest solar energy, Photosynth. Res. 81 (2004) 207–214.
[101] W. Kühlbrandt, Many wheels make light work, Nature 374 (1995) 497.
[102] J. Deisenhofer, O. Epp, K. Miki, R. Huber, H. Michel, X-ray structure analysis of a membrane protein complex, J. Mol. Biol. 180 (1984) 385–398.
[103] C.R. Lancaster, M. Bibikova, P. Sabatino, D. Oesterheld, H. Michel, Structural basis of the drastically increased initial electron transfer rate in the reaction center from a *Rhodopseudomonas viridis* mutant described at 2.0 Å resolution, J. Biol. Chem. 275 (2000) 39364–39368.
[104] J. Deisenhofer, H. Michel, NOBEL LECTURE: the photosynthetic reaction centre from the purple bacterium *Rhodopseudomonas viridis*, EMBO J. 8 (1989) 2149–2170.
[105] J. Deisenhofer, O. Epp, I. Sinning, H. Michel, Crystallographic refinement at 2.3 Å resolution and refined model of the photosynthetic reaction centre from *Rhodopseudomonas viridis*, J. Mol. Biol. 246 (1995) 429–457.
[106] G. Montoya, M. Cyrklaff, I. Sinning, Two-dimensional crystallization and preliminary structure analysis of light harvesting II (B800–850) complex from the purple bacterium *Rhodovulum sulfidophilum*, J. Mol. Biol. 250 (1995) 1–10.
[107] K.R. Miller, Three-dimensional structure of a photosynthetic membrane, Nature 300 (1982) 53–55.
[108] G. Kurisu, H. Zhang, J.L. Smith, W.A. Cramer, Structure of the cytochrome b6f complex of oxygenic photosynthesis: tuning the cavity, Science 302 (2003) 1009–1014.
[109] D. Stroebel, Y. Choquet, J.L. Popot, D. Picot, An atypical haem in the cytochrome b(6)f complex, Nature 426 (2003) 413–418.
[110] E.A. Berry, L.-S. Huang, L.K. Saechao, N.G. Pon, M. Valkova-Valchanova, F. Daldal, X-ray structure of *Rhodobacter capsulatus* cytochrome bc1: comparison with its mitochondrial and chloroplast counterparts, Photosynth. Res. 81 (2004) 251–275.
[111] M.Z. Papiz, S.M. Prince, A.M. Hawthornthwaite-Lawless, G. McDermott, A.A. Freer, N.W. Isaacs, R.J. Cogdell, A model for the photosynthetic apparatus of purple bacteria, Trends Plant Sci. 1 (1996) 198–206.
[112] X. Hu, A. Damjanovic, T. Ritz, K. Schulten, Architecture and mechanism of the light-harvesting apparatus of purple bacteria, Proc. Natl. Acad. Sci. U. S. A. 95 (1998) 5935–5941.
[113] R.N. Frese, J.D. Olsen, R. Branvall, W.H. Westerhuis, C.N. Hunter, R. van Grondelle, The long-range supraorganization of the bacterial photosynthetic unit: a key role for PufX, Proc. Natl. Acad. Sci. U. S. A. 97 (2000) 5197–5202.
[114] W. Kühlbrandt, Two-dimensional crystallization of membrane proteins, Q. Rev. Biophys. 25 (1992) 1–25.
[115] J. Rigaud, M. Chami, O. Lambert, D. Lévy, J. Ranck, Use of detergents in two-dimensional crystallization of membrane proteins, Biochim. Biophys. Acta 23 (2000) 112–128.
[116] R.A. Brunisholz, F. Suter, H. Zuber, Structural and spectral characterization of the antenna complexes of *Rhodocyclus gelatinosus*. Indication of a hair-pin-like arranged antenna apoprotein with an unusually high alanine content, Eur. J. Biochem. 222 (1994) 667–675.
[117] G. Drews, R.A. Niederman, Membrane biogenesis in anoxygenic photosynthetic prokaryotes, Photosynth. Res. 73 (2002) 87–94.
[118] K.R. Miller, J.S. Jacob, The *Rhodopseudomonas viridis* photosynthetic membrane: arrangement in situ, Arch. Microbiol. 142 (1985) 333–339.
[119] G. Drews, J.R. Golecki, in: R.E. Blankenship, M.T. Madigan, C.E. Bauer (Eds.), Anoxygenic photosynthetic bacteria, Kluwer Academic Publishers, Netherlands, 1995, pp. 231–257.
[120] W. Stark, W. Kühlbrandt, I. Wildhaber, E. Wehrli, K. Muhlethaler, The structure of the photoreceptor unit of *Rhodopseudomonas viridis*, EMBO J. 3 (1984) 777–783.
[121] I. Ikeda-Yamasaki, T. Odahara, K. Mitsuoka, Y. Fujiyoshi, K. Murata, Projection map of the reaction center-light harvesting 1 complex from *Rhodopseudomonas viridis* at 10 Å resolution, FEBS Lett. 425 (1998) 505–508.
[122] W. Barz, F. Francia, G. Venturoli, B. Melandri, A. Vermeglio, D. Oesterheld, Role of PufX protein in photosynthetic growth of *Rhodobacter sphaeroides*. 1. PufX is required for efficient light-driven electron transfer and photophosphorylation under anaerobic conditions, Biochemistry 34 (1995) 15235–15247.
[123] W. Barz, A. Vermeglio, F. Francia, G. Venturoli, B. Melandri, D. Oesterheld, Role of the PufX protein in the photosynthetic growth of *Rhodobacter sphaeroides*. 2. PufX is required for efficient ubiquinone/ubiquinol exchange between the reaction center QB site and the cytochrome bc1 complex, Biochemistry 34 (1995) 15248–15258.
[124] F. Francia, J. Wang, G. Venturoli, B. Melandri, W. Barz, D. Oesterheld, The reaction center-LH1 antenna complex of *Rhodobacter sphaeroides* contains one PufX molecule which is involved in dimerization of this complex, Biochemistry 38 (1999) 6834–6845.
[125] C.A. Siebert, P. Qian, D. Fotiadis, A. Engel, C.N. Hunter, P.A. Bullough, Molecular architecture of photosynthetic membranes in *Rhodobacter sphaeroides*: the role of PufX, EMBO J. 23 (2004) 690–700.
[126] R.N. Frese, C.A. Siebert, R.A. Niederman, C.N. Hunter, C. Otto, R. van Grondelle, The long-range organization of a native photosynthetic membrane, Proc. Natl. Acad. Sci. U. S. A. 101 (2004) 17994–17999.
[127] F. Francia, M. Dezi, A. Rebecchi, A. Mallardi, G. Palazzo, B.A. Melandri, G. Venturoli, Light-harvesting complex 1 stabilizes P+QB− charge separation in reaction centers of *Rhodobacter sphaeroides*, Biochemistry 43 (2004) 14199–14210.
[128] F. Comayras, C. Jungas, J. Lavergne, Functional consequences of the organization of the photosynthetic apparatus in *R. sphaeroides*: 1. Quinone domains and excitation transfer in chromatophores and reaction center–antenna complexes, J. Biol. Chem. 280 (2005) 11203–11213.
[129] F. Comayras, C. Jungas, J. Lavergne, Functional consequences of the organization of the photosynthetic apparatus in *R. sphaeroides*: 2. A study of PufX-membranes, J. Biol. Chem. 80 (2005) 11214–11223.
[130] P. Joliot, A. Vermeglio, A. Joliot, Evidence for supercomplexes between reaction centers, cytochrome *c*2 and cytochrome bc1 complex in *Rhodobacter sphaeroides* whole cells, Biochim. Biophys. Acta 975 (1989) 336–345.
[131] A. Vermeglio, P. Joliot, The photosynthetic apparatus of *Rhodobacter sphaeroides*, Trends Microbiol. 7 (1999) 435–440.
[132] A. Vermeglio, P. Joliot, Supramolecular organization of the photosynthetic chain in anoxygenic bacteria, Biochim. Biophys. Acta 1555 (2002) 60–64.